Article

Trigonometric Solution for the Bending Analysis of Magneto-Electro-Elastic Strain Gradient Nonlocal Nanoplates in Hygro-Thermal Environment

Giovanni Tocci Monaco [1,2], Nicholas Fantuzzi [1,*], Francesco Fabbrocino [3] and Raimondo Luciano [2]

[1] DICAM Department, University of Bologna, 40136 Bologna, Italy; giovanni.toccimonaco@studio.unibo.it
[2] Engineering Department, Parthenope University, 80133 Naples, Italy; raimondo.luciano@uniparthenope.it
[3] Department of Engineering, Telematic University Pegaso, 80133 Naples, Italy; francesco.fabbrocino@unipegaso.it
[*] Correspondence: nicholas.fantuzzi@unibo.it

Abstract: Nanoplates have been extensively utilized in the recent years for applications in nanoengineering as sensors and actuators. Due to their operative nanoscale, the mechanical behavior of such structures might also be influenced by inter-atomic material interactions. For these reasons, nonlocal models are usually introduced for studying their mechanical behavior. Sensor technology of plate structures should be formulated with coupled mechanics where elastic, magnetic and electric fields interact among themselves. In addition, the effect of hygro-thermal environments are also considered since their presence might effect the nanoplate behavior. In this work a trigonometric approach is developed for investigating smart composite nanoplates using a strain gradient nonlocal procedure. Convergence of the present method is also reported in terms of displacements and electro-magnetic potentials. Results agree well with the literature and open novel applications in this field for further developments.

1. Introduction

Recently, great attention has been paid to nanostructures composed of materials with magneto-electro-thermo-elasitc (METE) properties, with a main focus on the magneto-electro-thermo-mechanical coupling effects. Due to their properties, these materials have an important role in nano- and micro-electro-mechanical systems (NEMS and MEMS), such as sensors, actuators and transducers [1–4]. The fields of use of these devices are many and range from medicine to aerospace and civil engineering [5–10]. Generally, graphene is the main component of these devices since it is well-known for its stunning electro-mechanical properties [11].

Due to the high computational cost of atomic models, more and more mechanical theories are being investigated to predict the nanoscale effects for small-scale structures [12,13] by using simpler structural theories. These small-scale structures show mechanical size-dependency in experiments and atomistic simulations [14,15], therefore, classical continuum theories need to be modified to take the small-scale effect into account [16]. Nonlocal theories have been widely used for the study of nanostructures since Eringen developed his theory of nonlocal elasticity [17], which considers the nanoscale effects by introducing one or more length scale parameters in addition to the well-known linear elastic Lamé parameters. [18–21]. Nonlocal theories are generally presented as—strain gradient [22–25], stress gradient [26], modified strain gradient [27–29], couple stress [30], modified couple stress [31,32], integral type [33,34] and micropolar [35–37]. Among others nanobeams [38] and stress-driven nonlocal integral elasticity has been investigated in [39].

METE material properties and structures have been extensively studied in recent years due to the ever-increasing nanoengineering applications. A matrix method for evaluating effective elastic constants of generally anisotropic multilayered composites with various coupled physical effects including piezoelectricity, piezomagnetism, thermoelasticity has been presented in [40]. Malikan et al. [41] presented the instabilities and post-buckling behavior of piezomagnetic and flexomagnetic for Bernoulli-Euler type nanostructures. In [42] a homogenization micromechanical method for the prediction of the effective moduli of electro-magneto-thermo-elastic composites was developed. Vinyas et al. in [43,44] investigated the effect of the particle arrangement on the static response of magneto-electro-thermo-elastic plates composed by $BaTiO_3$–$CoFe_2O_4$ using a finite element formulation. In [45] the effects of different molar ratio on the microstructure, dielectric and electromagnetic properties of $BaTiO_3$–$CoFe_2O_4$ ceramic were investigated experimentally. In [46], the pyroelectric and pyromagnetic effects on the behavior of METE plate under different boundary conditions subjected to uniform temperature is studied. Bacciocchi et al. [47] developed a finite element solution for the static behavior of laminated nanoplates in a hygro-thermal environment, taking into account the effect of material length scales, which is described by the nonlocal strain gradient theory. Static and dynamic analyses of macro and nano functionally graded (FG) plates was studied using exact three-dimensional elasticity considering thermal effects in [48]. FG thin structures have recently been presented in [49,50] for static and dynamic analysis when the inhomogeneity is present at the structural midsurface. Functionally graded structures with and without electro-magnetic effects have been investigated for rectangular microplates [51,52] and circular plates [53–55] also. The static and dynamic problems for thin and thick METE plates were studied by using a third order shear deformation theory and the solution was obtained via finite element method in [56] and via Navier's solution method in [57]. Magneto-electro elastic effects in Functionally Graded Materials (FGM) nanoplates were considered in [58]. In [59], bending and buckling analyses of $BaTiO_3$–$CoFe_2O_4$ nanoplates based on nonlocal strain gradient and modified couple stress are developed. In [60], the thermo-electro-mechanical bending behavior of a sandwich nanoplate integrated with two piezoelectric face sheets was studied using the trigonometric shear and normal deformations plate theory. In [61], the free vibration of magneto-electro-elastic nanoplates was investigated based on the nonlocal strain gradient theory and Kirchhoff plate theory and considering thermal environment. Gholami et al. in [62] present higher-order shear deformable plate model for METE rectangular nanoplates by adopting the nonlocal elasticity theory and Navier's solution method. In [63–65] a nonlocal nonlinear first-order shear theory is used for investigating the buckling and free vibration of METE nanoplates under magneto-electro-thermo-mechanical loads. Mota in [66] investigated the influence of the shear correction factor used in the context of the first-order shear deformation theory on FG porous materials. Brischetto et al. [67] analyzed the deformations of a simply supported, functionally graded, rectangular plate subjected to thermo-mechanical loads using Carrera unified formulation. Again, Brischetto and Carrera [68] investigated coupled thermo-electro-mechanical effects of smart plates. In [69] an exact solution of static behavior for nanobeams and nanoplates based on nonlocal elasticity theory is provided. It is worth to mention recent contributions in the flexo- and piezo-magnetic properties of nanobeams [70] and structures [71]. As well as hygro-thermo-electro-mechanical coupling effects of beams [72].

The focus of this paper is the study of the static behavior of functionally graded nanoplates subjected to mechanical, electrical and magnetic loads in a hygro-thermal environment through the use of nonlocal strain gradient theory. After the present introductory section, the paper is structured as follows. First, the fundamental equations governing the problem of functionally graded (FG) thin plates in a hygro-thermal environment, considering piezo-magnetic coupling terms, are described and the governing equation are carried out via principle of virtual work. The equations above include nonlocal effects by considering the strain gradient theory. Electric and magnetic fields will be approximated

by considering the satisfaction of Maxwell equations. Second, the trigonometric solution is described according to Navier expansion and carried out in algebraic form. Finally, numerical results are presented by varying mechanical loads and electro-magnetic density loads. All computations have been performed using a MATLAB code. In the last section, final considerations and remarks are given in order to describe the most important effects observed for the present problem.

2. Theoretical Background

In the following, a magneto-electro-thermo-elastic (METE) rectangular thin nanoplate is considered. A plate sketch is depicted in Figure 1, where its in-plane size *a*, *b* and thickness *h* are indicated according to a Cartesian reference system (x, y, z) [73].
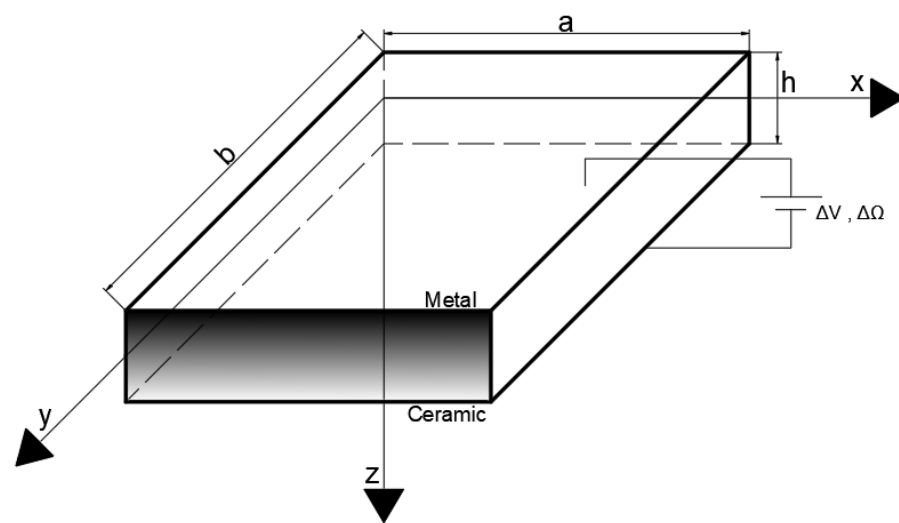
Figure 1. Functionally graded plate with applied electric ΔV and magnetic potentials $\Delta \Omega$.

In the present problem formulation, the METE nanoplate interacts with a hygro-thermal environment together with electro-magnetic potentials (ΔV and $\Delta \Omega$, respectively) applied between the top and bottom surfaces of the plate (please note note vertical axis points down so the bottom surface is the one for $z = -h/2$ and the top surface is identified by $z = h/2$).

The displacement field considered in the present work is the one according to Kirchhoff theory [73] where the in-plane displacements are *u*,*v* and the transverse motion is indicated by *w*. At present, the constitutive equations for the present problem can be reported in matrix form as

$$\sigma = \mathbf{C}\varepsilon - \mathbf{e}\mathbf{E} - \mathbf{q}\mathbf{H} - \mathbf{C}\alpha\Delta T - \mathbf{C}\beta\Delta C$$
$$\mathbf{D}_E = \mathbf{e}^\top\varepsilon + \xi\mathbf{E} + \zeta\mathbf{H} - \mathbf{p}\Delta T - \mathbf{h}\Delta C \qquad (1)$$
$$\mathbf{B}_M = \mathbf{q}^\top\varepsilon + \zeta\mathbf{E} + \chi\mathbf{H} - \lambda\Delta T - \eta\Delta C,$$

in which σ is the classical stress vector including σ_i for $i = 1, 2, \ldots, 6$ (according to Voigt-Kelvin notation [74]). $\mathbf{D}_E = [D_x, D_y, D_z]^\top$ and $\mathbf{B}_M = [B_x, B_y, B_z]^\top$ are the electrical displacement and magnetic flux vectors, respectively. ε is the classical strain vector including ε_i for $i = 1, 2, \ldots, 6$. $\mathbf{E} = [E_1, E_2, E_3]^\top$ and $\mathbf{H} = [H_1, H_2, H_3]^\top$ are the electric and magnetic field vectors respectively. $\mathbf{C}$ is the classical stiffness matrix including C_{ij} for $i, j = 1, 2, \ldots, 6$. ξ and χ represent the electrical and magnetic permittivity matrices, respectively. Piezo-electric and piezo-magnetic properties are included in the matrices $\mathbf{e}$, $\mathbf{q}$, respectively, which in general include 18 independent coefficients. Magneto-electro-elastic

(MEE) properties are given by ζ. Finally, pyro-electric $\mathbf{p}$, pyro-magnetic λ, hygro-electric $\mathbf{h}$ and hygro-magnetic η are introduced to take into account the hygro-thermal effect on the electric and magnetic fields. It is mentioned that hygro-thermal effects for the elastic part are given by α and β, respectively.

For the stress plane state assumption ($\sigma_3 = 0$), the normal strain ε_3 can be carried out and condensed in the other quantities. Then, the constitutive equations in the case of orthotropic material and the stress plane state can therefore be rewritten as follows

$$
\begin{aligned}
\sigma_1 &= \left(C_{11} - \frac{C_{13}^2}{C_{33}} \right) \varepsilon_1 + \left(C_{12} - C_{13}\frac{C_{23}}{C_{33}} \right) \varepsilon_2 - \left(e_{31} - C_{13}\frac{e_{33}}{C_{33}} \right) E_3 - \left(q_{31} - C_{13}\frac{q_{33}}{C_{33}} \right) H_3 \\
&\quad - \left[\left(C_{11} - \frac{C_{13}^2}{C_{33}} \right)\alpha_1 + \left(C_{12} - C_{13}\frac{C_{23}}{C_{33}} \right)\alpha_2 \right] \Delta T - \left[\left(C_{11} - \frac{C_{13}^2}{C_{33}} \right)\beta_1 + \left(C_{12} - C_{13}\frac{C_{23}}{C_{33}} \right)\beta_2 \right] \Delta C \\
&= Q_{11}\varepsilon_1 + Q_{12}\varepsilon_2 - \tilde{e}_{31}E_3 - \tilde{q}_{31}H_3 - (Q_{11}\alpha_1 + Q_{12}\alpha_2)\Delta T - (Q_{11}\beta_1 + Q_{12}\beta_2)\Delta C,
\end{aligned}
\tag{2}
$$

similarly for σ_2 it will be

$$
\sigma_2 = Q_{12}\varepsilon_1 + Q_{22}\varepsilon_2 - \tilde{e}_{32}E_3 - \tilde{q}_{32}H_3 - (Q_{12}\alpha_1 + Q_{22}\alpha_2)\Delta T - (Q_{12}\beta_1 + Q_{22}\beta_2)\Delta C \tag{3}
$$

D_z can be written as

$$
\begin{aligned}
D_z &= \left(e_{31} - e_{33}\frac{C_{13}}{C_{33}} \right)\varepsilon_1 + \left(e_{32} - e_{33}\frac{C_{23}}{C_{33}} \right)\varepsilon_2 + \left(\xi_{33} + \frac{e_{33}^2}{C_{33}} \right)E_3 + \left(\zeta_{33} + e_{33}\frac{q_{33}}{C_{33}} \right)H_3 \\
&\quad - \left(p_3 - \frac{C_{13}}{C_{33}}\alpha_1 - \frac{C_{23}}{C_{33}}\alpha_2 \right)\Delta T - \left(h_3 - \frac{C_{13}}{C_{33}}\beta_1 - \frac{C_{23}}{C_{33}}\beta_2 \right)\Delta C \\
&= \tilde{e}_{31}\varepsilon_1 + \tilde{e}_{32}\varepsilon_2 + \tilde{\xi}_{33}E_3 + \tilde{\zeta}_{33}H_3 - \tilde{p}_3\Delta T - \tilde{h}_3\Delta C,
\end{aligned}
\tag{4}
$$

and, similarly, B_z will be

$$
B_z = \tilde{q}_{31}\varepsilon_1 + \tilde{q}_{32}\varepsilon_2 + \tilde{\zeta}_{33}E_3 + \tilde{\chi}_{33}H_3 - \tilde{\lambda}_3\Delta T - \tilde{\eta}_3\Delta C. \tag{5}
$$

So the piezo-magnetic quantities defined in Equation (1) take the following reduced form

$$
\begin{aligned}
\tilde{\mathbf{e}} &= \begin{bmatrix} 0 & 0 & \tilde{e}_{31} \\ 0 & 0 & \tilde{e}_{32} \\ 0 & 0 & 0 \end{bmatrix}, \quad
\tilde{\mathbf{q}} = \begin{bmatrix} 0 & 0 & \tilde{q}_{31} \\ 0 & 0 & \tilde{q}_{32} \\ 0 & 0 & 0 \end{bmatrix}, \quad
\tilde{\xi} = \begin{bmatrix} \xi_1 & 0 & 0 \\ 0 & \xi_2 & 0 \\ 0 & 0 & \tilde{\xi}_3 \end{bmatrix}, \quad
\tilde{\chi} = \begin{bmatrix} \chi_1 & 0 & 0 \\ 0 & \chi_2 & 0 \\ 0 & 0 & \tilde{\chi}_3 \end{bmatrix}, \\
\tilde{\zeta} &= \begin{bmatrix} \zeta_1 & 0 & 0 \\ 0 & \zeta_2 & 0 \\ 0 & 0 & \tilde{\zeta}_3 \end{bmatrix}, \quad
\mathbf{p} = \begin{Bmatrix} p_1 \\ p_2 \\ \tilde{p}_3 \end{Bmatrix}, \quad
\lambda = \begin{Bmatrix} \lambda_1 \\ \lambda_2 \\ \tilde{\lambda}_3 \end{Bmatrix}, \quad
\mathbf{h} = \begin{Bmatrix} h_1 \\ h_2 \\ \tilde{h}_3 \end{Bmatrix}, \quad
\eta = \begin{Bmatrix} \eta_1 \\ \eta_2 \\ \tilde{\eta}_3 \end{Bmatrix}.
\end{aligned}
\tag{6}
$$

Differently from the classical continuum theory (e.g., Cauchy), nonlocal strain gradient theory expresses that the stress at a point is not only a linear function of the strains but also of the second gradient of the same. For this reason, the classical constitutive Equation (1) for functionally graded materials can be reported in the form

$$
\sigma(x,y,z) = \left(1 - \ell^2\nabla^2 \right)\left[\mathbf{Q}(z)\varepsilon - \tilde{\mathbf{e}}(z)\mathbf{E} - \tilde{\mathbf{q}}(z)\mathbf{H} \right] - \mathbf{Q}(z)\alpha(z)\Delta T - \mathbf{Q}(z)\beta(z)\Delta C
$$

$$
\mathbf{D}_E(x,y,z) = \left(1 - \ell^2\nabla^2 \right)\left[\tilde{\mathbf{e}}^\top(z)\varepsilon + \tilde{\xi}(z)\mathbf{E} + \tilde{\zeta}(z)\mathbf{H} \right] - \mathbf{p}(z)\Delta T - \mathbf{h}(z)\Delta C \tag{7}
$$

$$
\mathbf{B}_M(x,y,z) = \left(1 - \ell^2\nabla^2 \right)\left[\tilde{\mathbf{q}}^\top(z)\varepsilon + \tilde{\zeta}(z)\mathbf{E} + \tilde{\chi}(z)\mathbf{H} \right] - \lambda(z)\Delta T - \eta(z)\Delta C,
$$

where ℓ is the nonlocal parameter, $\nabla^2 = \partial^2/\partial x^2 + \partial^2/\partial y^2$ is the Laplacian and the dependency on the z coordinate is explicitly given. Please note that the stress and strain vectors

in Equation (7) have 5 components because one has been reduced according to what has been previously reported.

In addition, it is recalled that electric and magnetic fields depend on the Cartesian coordinates (x, y, z) and hygro-thermal variations are assumed to have a linear variation along the thickness [75] as

$$\Delta T(x,y,z) = T_0(x,y) + \frac{z}{h}T_1(x,y), \quad \Delta C(x,y,z) = C_0(x,y) + \frac{z}{h}C_1(x,y), \tag{8}$$

where $T_0(x,y)$ and $C_0(x,y)$ represent a constant temperature and moisture concentration whereas $T_1(x,y)$ and $C_1(x,y)$ indicate a linear temperature and moisture concentration variation on the plate middle surface. It is noted that $T_0(x,y)$ and $T_1(x,y)$ are described by the same units (e.g., temperature), analogously $C_0(x,y)$ and $C_1(x,y)$ (e.g., moisture concentration).

2.1. Electric and Magnetic Potentials

The following assumption is considered for the magnetic and electric fields

$$\Phi(x,y,z) = -\cos\frac{\pi z}{h}\phi(x,y) + \frac{2z}{h}\Delta V$$

$$Y(x,y,z) = -\cos\frac{\pi z}{h}\gamma(x,y) + \frac{2z}{h},\Delta \Omega \tag{9}$$

where ϕ, γ represent the parameters for the electric and magnetic potentials in closed-circuit configuration, respectively. ΔV and $\Delta \Omega$ indicate the applied electric and magnetic potentials in open-circuit configuration, respectively. Therefore, in this work a combination of cosinusoidal and linear variations are taken into account and such selection satisfy the Maxwell equations for the present problem [76]. It is convenient to report the electric and magnetic fields in matrix form as shown below

$$\mathbf{E} = \nabla\Phi = \mathbf{f}_E\mathbb{D}_E\phi + \mathbf{E}_0, \quad \mathbf{H} = \mathbf{f}_H\mathbb{D}_H\gamma + \mathbf{H}_0, \tag{10}$$

where

$$\mathbf{f}_E = \mathbf{f}_H = \begin{bmatrix} \cos\frac{\pi z}{h} & 0 & 0 \\ 0 & \cos\frac{\pi z}{h} & 0 \\ 0 & 0 & -\frac{\pi}{h}\sin\frac{\pi z}{h} \end{bmatrix}, \quad \mathbb{D}_E = \mathbb{D}_H = \begin{Bmatrix} \frac{\partial}{\partial x} \\ \frac{\partial}{\partial y} \\ 1 \end{Bmatrix}$$

$$\mathbf{E}_0 = \begin{Bmatrix} 0 \\ 0 \\ -\frac{2}{h}\Delta V \end{Bmatrix}, \quad \mathbf{H}_0 = \begin{Bmatrix} 0 \\ 0 \\ -\frac{2}{h}\Delta\Omega \end{Bmatrix} \tag{11}$$

2.2. Balance Equations

The principle of virtual work $\delta H_{ent} + \delta V = 0$ is used to carry out the balance equations, where δH_{ent} is the variation of enthalpy and δV is the external potential done by applied forces. The variation of enthalpy reads

$$\delta H_{ent} = \int_{\mathcal{A}}\int_{-\frac{h}{2}}^{\frac{h}{2}}\Big\{\sigma_{xx}\delta\varepsilon_{xx} + \sigma_{yy}\delta\varepsilon_{yy} + \sigma_{xy}\delta\gamma_{xy}$$

$$- (D_x\delta E_x + D_y\delta E_y + D_z\delta E_z + B_x\delta H_x + B_y\delta H_y + B_z\delta H_z)\Big\}dzd\mathcal{A}, \tag{12}$$

integrating along the thickness the classical stress resultants $N_{xx}, N_{yy}, N_{xy}, M_{xx}, M_{yy}, M_{xy}$ should be introduced [77]. Moreover by defining the following quantities

$$\begin{Bmatrix} \mathcal{D}_x \\ \mathcal{D}_y \\ \mathcal{D}_z \end{Bmatrix} = \int_{-\frac{h}{2}}^{\frac{h}{2}} \mathbf{f}_E\mathbf{D}_E \, dz, \quad \begin{Bmatrix} \mathcal{B}_x \\ \mathcal{B}_y \\ \mathcal{B}_z \end{Bmatrix} = \int_{-\frac{h}{2}}^{\frac{h}{2}} \mathbf{f}_B\mathbf{B}_M \, dz \tag{13}$$

it is obtained

$$
\begin{aligned}
\delta H_{ent} = \int_{\mathcal{A}} \Bigg\{ & N_{xx}\left(\frac{\partial \delta u}{\partial x} + \frac{\partial w}{\partial x}\frac{\partial \delta w}{\partial x} \right) + N_{yy}\left(\frac{\partial \delta v}{\partial y} + \frac{\partial w}{\partial y}\frac{\partial \delta w}{\partial y} \right) \\
& + N_{xy}\left(\frac{\partial \delta u}{\partial y} + \frac{\partial \delta v}{\partial x} + \frac{\partial \delta w}{\partial y}\frac{\partial w}{\partial x} + \frac{\partial \delta w}{\partial x}\frac{\partial w}{\partial y} \right) + \\
& + M_{xx}\left(-\frac{\partial^2 \delta w}{\partial x^2} \right) + M_{yy}\left(-\frac{\partial^2 \delta w}{\partial y^2} \right) + M_{xy}\left(-2\frac{\partial^2 \delta w}{\partial x \partial y} \right) + \\
& -\left(\mathcal{D}_x \frac{\partial \delta \phi}{\partial x} + \mathcal{D}_y \frac{\partial \delta \phi}{\partial y} + \mathcal{D}_x \delta \phi + \mathcal{B}_x \frac{\partial \delta \gamma}{\partial x} + \mathcal{B}_y \frac{\partial \delta \gamma}{\partial y} + \mathcal{B}_z \delta \gamma \right) \Bigg\} d\mathcal{A}.
\end{aligned}
\tag{14}
$$

Integrating by parts Equation (14) the enthalpy becomes

$$
\begin{aligned}
\delta H_{ent} = \int_{\mathcal{A}} \Bigg\{ & \left(\frac{\partial N_{xx}}{\partial x} + \frac{\partial N_{xy}}{\partial y} \right)\delta u + \left(\frac{\partial N_{xy}}{\partial x} + \frac{\partial N_{yy}}{\partial y} \right)\delta v + \left[\frac{\partial}{\partial x}\left(N_{xx}\frac{\partial w}{\partial x} + N_{xy}\frac{\partial w}{\partial y} \right) \right. \\
& \left. + \frac{\partial}{\partial y}\left(N_{xy}\frac{\partial w}{\partial x} + N_{yy}\frac{\partial w}{\partial y} \right) + \frac{\partial^2 M_{xx}}{\partial x^2} + \frac{\partial^2 M_{yy}}{\partial y^2} + 2\frac{\partial^2 M_{xy}}{\partial x \partial y} \right]\delta w \\
& -\left(\frac{\partial \mathcal{D}_x}{\partial x} + \frac{\partial \mathcal{D}_y}{\partial y} + \mathcal{D}_z \right)\delta \phi - \left(\frac{\partial \mathcal{B}_x}{\partial x} + \frac{\partial \mathcal{B}_y}{\partial y} + \mathcal{B}_z \right)\delta \gamma \Bigg\} d\mathcal{A} + \\
& -\int_{\Gamma} \Bigg\{ (N_{xx}\, n_x + N_{xy}\, n_y)\delta u + (N_{xy}\, n_x + N_{yy}\, n_y)\delta v + \Big[(N_{xx}n_x + N_{xy}n_y)\frac{\partial w}{\partial x} \\
& + (N_{xy}n_x + N_{yy}n_y)\frac{\partial w}{\partial y} + \left(\frac{\partial M_{xx}}{\partial x} + \frac{\partial M_{xy}}{\partial y} \right)n_x + \left(\frac{\partial M_{yy}}{\partial y} + \frac{\partial M_{xy}}{\partial x} \right)n_y \Big]\delta w \\
& - (M_{xx}n_x + M_{xy}n_y)\frac{\partial \delta w}{\partial x} - (M_{xy}n_x + M_{yy}n_y)\frac{\partial \delta w}{\partial y} \\
& - (\mathcal{D}_x\, n_x + \mathcal{D}_y\, n_y)\delta \phi - (\mathcal{B}_x\, n_x + \mathcal{B}_y\, n_y)\delta \gamma \Bigg\} d\Gamma
\end{aligned}
\tag{15}
$$

The potential due to external actions takes the form

$$
\begin{aligned}
\delta V = \int_{\mathcal{A}} \Bigg\{ & q\delta w + \rho_E \delta \phi + \rho_H \delta \gamma \Bigg\} d\mathcal{A} + \int_{\Gamma} \Bigg\{ (\hat{N}_{xx}\, n_x + \hat{N}_{xy}\, n_y)\delta u \\
& + (\hat{N}_{xy}\, n_x + \hat{N}_{yy}\, n_y)\delta v - (\hat{M}_{xx}\, n_x + \hat{M}_{xy}\, n_y)\frac{\partial \delta w}{\partial x} \\
& - (\hat{M}_{xy}\, n_x + \hat{M}_{yy}\, n_y)\frac{\partial \delta w}{\partial y} + (\hat{Q}_x + \hat{Q}_y)\delta w \Bigg\} d\Gamma
\end{aligned}
\tag{16}
$$

where ρ_E represents the electric charge density and ρ_H the electric current density, also referred to as the magnetic charge density for comparison with the electric field. By introducing $\mathcal{N}(w)$ and $\mathcal{P}(w)$ as

$$
\begin{aligned}
\mathcal{N}(w) &= \frac{\partial}{\partial x}\left(N_{xx}\frac{\partial w}{\partial x} + N_{xy}\frac{\partial w}{\partial y} \right) + \frac{\partial}{\partial y}\left(N_{xy}\frac{\partial w}{\partial x} + N_{yy}\frac{\partial w}{\partial y} \right) \\
\mathcal{P}(w) &= \left(N_{xx}\frac{\partial w}{\partial x} + N_{xy}\frac{\partial w}{\partial y} \right)n_x + \left(N_{xy}\frac{\partial w}{\partial x} + N_{yy}\frac{\partial w}{\partial y} \right)n_y.
\end{aligned}
\tag{17}
$$

The balance equations can be written as follows

$$\frac{\partial N_{xx}}{\partial x} + \frac{\partial N_{xy}}{\partial y} = 0$$

$$\frac{\partial N_{yy}}{\partial y} + \frac{\partial N_{xy}}{\partial x} = 0$$

$$\frac{\partial^2 M_{xx}}{\partial x^2} + 2\frac{\partial^2 M_{xy}}{\partial x \partial y} + \frac{\partial^2 M_{yy}}{\partial y^2} + \mathcal{N}(w) = -q \tag{18}$$

$$\frac{\partial \mathcal{D}_x}{\partial x} + \frac{\partial \mathcal{D}_y}{\partial y} + \mathcal{D}_z = -\rho_E$$

$$\frac{\partial \mathcal{B}_x}{\partial x} + \frac{\partial \mathcal{B}_y}{\partial y} + \mathcal{B}_z = -\rho_H$$

and the boundary conditions become

$$\delta u = 0 \quad \text{or} \quad \left(N_{xx} - \hat{N}_{xx}\right)n_x + \left(N_{xy} - \hat{N}_{xy}\right)n_y = 0$$

$$\delta v = 0 \quad \text{or} \quad \left(N_{yy} - \hat{N}_{yy}\right)n_y + \left(N_{xy} - \hat{N}_{xy}\right)n_x = 0$$

$$\delta w = 0 \quad \text{or} \quad \left(\frac{\partial M_{xx}}{\partial x} + \frac{\partial M_{xy}}{\partial y}\right)n_x +$$

$$+ \left(\frac{\partial M_{yy}}{\partial y} + \frac{\partial M_{xy}}{\partial x}\right)n_y + \mathcal{P}(w) - \left(\hat{Q}_x + \hat{Q}_y\right) = 0 \tag{19}$$

$$\frac{\partial \delta w}{\partial x} = 0 \quad \text{or} \quad \left(M_{xx} - \hat{M}_{xx}\right)n_x + \left(M_{xy} - \hat{M}_{xy}\right)n_y = 0$$

$$\frac{\partial \delta w}{\partial y} = 0 \quad \text{or} \quad \left(M_{yy} - \hat{M}_{yy}\right)n_y + \left(M_{xy} - \hat{M}_{xy}\right)n_x = 0$$

$$\delta \phi = 0 \quad \text{or} \quad \mathcal{D}_x \, n_x + \mathcal{D}_y \, n_y = 0$$

$$\delta \gamma = 0 \quad \text{or} \quad \mathcal{B}_x \, n_x + \mathcal{B}_y \, n_y = 0.$$

By including the constitutive equations in the equilibrium equations, the following equilibrium in terms of displacements and potentials can be carried out as

$$A_{11}\frac{\partial^2 u}{\partial x^2} + A_{12}\frac{\partial^2 v}{\partial x \partial y} + A_{66}\frac{\partial^2 u}{\partial y^2} + A_{66}\frac{\partial^2 v}{\partial x \partial y} - B_{11}\frac{\partial^3 w}{\partial x^3} - B_{12}\frac{\partial^3 w}{\partial x \partial y^2} - 2B_{66}\frac{\partial^3 w}{\partial x \partial y^2}$$

$$+ A^f_{E,13}\frac{\partial \phi}{\partial x} + A^f_{H,13}\frac{\partial \gamma}{\partial x} - A^\alpha_1\frac{\partial T_0}{\partial x} - \frac{B^\alpha_1}{h}\frac{\partial T_1}{\partial x} - A^\alpha_3\frac{\partial T_0}{\partial y} - \frac{B^\alpha_3}{h}\frac{\partial T_1}{\partial y} = 0 \tag{20}$$

$$A_{12}\frac{\partial^2 u}{\partial x \partial y} + A_{22}\frac{\partial^2 v}{\partial y^2} + A_{66}\frac{\partial^2 u}{\partial x \partial y} + A_{66}\frac{\partial^2 v}{\partial x^2} - B_{12}\frac{\partial^3 w}{\partial x^2 \partial y} - B_{22}\frac{\partial^3 w}{\partial y^3} - 2B_{66}\frac{\partial^3 w}{\partial x^2 \partial y}$$

$$+ A^f_{E,23}\frac{\partial \phi}{\partial y} + A^f_{H,23}\frac{\partial \gamma}{\partial y} - A^\alpha_2\frac{\partial T_0}{\partial y} - \frac{B^\alpha_2}{h}\frac{\partial T_1}{\partial y} - A^\alpha_3\frac{\partial T_0}{\partial x} - \frac{B^\alpha_3}{h}\frac{\partial T_1}{\partial x} = 0 \tag{21}$$

$$B_{11}\frac{\partial^3 u}{\partial x^3} + B_{12}\frac{\partial^3 v}{\partial x^2 \partial y} + B_{12}\frac{\partial^3 u}{\partial x \partial y^2} + B_{22}\frac{\partial^3 v}{\partial y^3} + 2B_{66}\frac{\partial^3 u}{\partial x \partial y^2} + 2B_{66}\frac{\partial^3 v}{\partial x^2 \partial y} - D_{11}\frac{\partial^4 w}{\partial x^4}$$

$$- 2D_{12}\frac{\partial^4 w}{\partial x^2 \partial y^2} - D_{22}\frac{\partial^4 w}{\partial y^4} - 4D_{66}\frac{\partial^4 w}{\partial x^2 \partial y^2} + B^f_{E,13}\frac{\partial^2 \phi}{\partial x^2} + B^f_{H,13}\frac{\partial^2 \gamma}{\partial x^2} + B^f_{E,23}\frac{\partial^2 \phi}{\partial y^2} \tag{22}$$

$$+ B^f_{H,23}\frac{\partial^2 \gamma}{\partial y^2} - B^\alpha_1\frac{\partial^2 T_0}{\partial x^2} - \frac{D^\alpha_1}{h}\frac{\partial^2 T_1}{\partial x^2} - B^\alpha_2\frac{\partial^2 T_0}{\partial y^2} - \frac{D^\alpha_2}{h}\frac{\partial^2 T_1}{\partial y^2} - 4B^\alpha_3\frac{\partial^2 T_0}{\partial x \partial y} - 4\frac{D^\alpha_3}{h}\frac{\partial T_1}{\partial x \partial y} = -q$$

$$B_{\xi,11}^f \frac{\partial^2 \phi}{\partial x^2} + B_{\zeta,11}^f \frac{\partial^2 \gamma}{\partial x^2} + B_{\xi,22}^f \frac{\partial^2 \phi}{\partial y^2} + B_{\zeta,22}^f \frac{\partial^2 \gamma}{\partial y^2} + B_{\xi,33}^f \phi + B_{\zeta,33}^f \gamma - A_{E,31}^f \frac{\partial u}{\partial x}$$

$$- A_{E,32}^f \frac{\partial v}{\partial y} - B_{E,31}^f \frac{\partial^2 w}{\partial x^2} - B_{E,32}^f \frac{\partial^2 w}{\partial y^2} - A_{p,1} \frac{\partial T_0}{\partial x} - \frac{B_{p,1}}{h} \frac{\partial T_1}{\partial x} - A_{p,2} \frac{\partial T_0}{\partial y} - \frac{B_{p,2}}{h} \frac{\partial T_1}{\partial y} \qquad (23)$$

$$+ A_{p,3} T_0 + \frac{B_{p,3}}{h} T_1 - A_{\xi,33}^f \frac{2}{h} \Delta V - A_{\zeta,33}^f \frac{2}{h} \Delta\Omega = -\rho_E$$

$$B_{\zeta,11}^f \frac{\partial^2 \phi}{\partial x^2} + B_{\chi,11}^f \frac{\partial^2 \gamma}{\partial x^2} + B_{\zeta,22}^f \frac{\partial^2 \phi}{\partial y^2} + B_{\chi,22}^f \frac{\partial^2 \gamma}{\partial y^2} + B_{\zeta,33}^f \phi + B_{\chi,33}^f \gamma - A_{H,31}^f \frac{\partial u}{\partial x}$$

$$- A_{H,32}^f \frac{\partial v}{\partial y} - B_{H,31}^f \frac{\partial^2 w}{\partial x^2} - B_{H,32}^f \frac{\partial^2 w}{\partial y^2} - A_{\lambda,1} \frac{\partial T_0}{\partial x} - \frac{B_{\lambda,1}}{h} \frac{\partial T_1}{\partial x} - A_{\lambda,2} \frac{\partial T_0}{\partial y} - \frac{B_{\lambda,2}}{h} \frac{\partial T_1}{\partial y} \qquad (24)$$

$$+ A_{\lambda,3} T_0 + \frac{B_{\lambda,3}}{h} T_1 - A_{\zeta,33}^f \frac{2}{h} \Delta V - A_{\chi,33}^f \frac{2}{h} \Delta\Omega = -\rho_H.$$

The present system of partial differential equations will be solved in the section below by using the Navier method.

3. Navier Solution

The Navier method is considered for obtaining a trigonometric solution of the problem. This choice allows us to solve the plate in simply-supported boundary conditions only; however, the quality of the solution is extremely fast and reliable and can be considered as a benchmark. Navier expansion for all the parameters governing the present problem takes the form

$$\begin{Bmatrix} u \\ v \\ w \\ \phi \\ \gamma \end{Bmatrix} = \sum_{m=1}^{\infty} \sum_{n=1}^{\infty} \begin{bmatrix} \cos\alpha x \sin\beta y & 0 & 0 & 0 & 0 \\ 0 & \sin\alpha x \cos\beta y & 0 & 0 & 0 \\ 0 & 0 & \sin\alpha x \sin\beta y & 0 & 0 \\ 0 & 0 & 0 & \sin\alpha x \sin\beta y & 0 \\ 0 & 0 & 0 & 0 & \sin\alpha x \sin\beta y \end{bmatrix} \begin{Bmatrix} U_{mn} \\ V_{mn} \\ W_{mn} \\ \Phi_{mn} \\ \Gamma_{mn}, \end{Bmatrix} \qquad (25)$$

where $\alpha = m\pi/a$ and $\alpha = n\pi/b$. A trigonometric expansion is also used for the mechanical and hygro-thermal loads as

$$(q, T_0, T_1, C_0, C_1) = \sum_{m=1}^{\infty} \sum_{n=1}^{\infty} (Q_{mn}, T_{0,mn}, T_{1,mn}, C_{0,mn}, C_{1,mn}) \sin\alpha x \sin\beta y. \qquad (26)$$

By substituting the displacements field into the equations of motion and performing the derivatives we obtain the following algebraic system which can be solved by using Cramer method.

$$\begin{bmatrix} \hat{c}_{11} & \hat{c}_{12} & \hat{c}_{13} & \hat{c}_{14} & \hat{c}_{15} \\ \hat{c}_{12} & \hat{c}_{22} & \hat{c}_{23} & \hat{c}_{24} & \hat{c}_{25} \\ \hat{c}_{13} & \hat{c}_{23} & \hat{c}_{33} + \tilde{s}_{33} & \hat{c}_{34} & \hat{c}_{35} \\ \hat{c}_{14} & \hat{c}_{24} & \hat{c}_{34} & \hat{c}_{44} & \hat{c}_{45} \\ \hat{c}_{15} & \hat{c}_{25} & \hat{c}_{35} & \hat{c}_{45} & \hat{c}_{55} \end{bmatrix} \begin{Bmatrix} U_{mn} \\ V_{mn} \\ W_{mn} \\ \Phi_{mn} \\ \Gamma_{mn} \end{Bmatrix} = \begin{Bmatrix} 0 \\ 0 \\ -Q_{mn} \\ -\rho_{E,mn} \\ -\rho_{H,mn} \end{Bmatrix} + \begin{Bmatrix} \mathcal{F}_{1,mn}^T \\ \mathcal{F}_{2,mn}^T \\ \mathcal{F}_{3,mn}^T \\ \mathcal{F}_{4,mn}^T \\ \mathcal{F}_{5,mn}^T. \end{Bmatrix} \qquad (27)$$

For the sake of conciseness, the coefficients $\hat{c}_{ij}$, $\tilde{s}_{33}$ and the vector $\mathcal{F}_{i,mn}^T$ for $i,j = 1, 2, \ldots, 5$ are defined in Appendix A Equations (A9) and (A10).

4. Applications

For the numerical applications, different functionally graded plates are considered. First a comparison with Reference [74] (Figure 2) is proposed where the plate is composed in the lower side of aluminium and in the upper side of zirconia. The properties of the two

materials are for the aluminium $E_{Al} = 70$ GPa, $v_{Al} = 0.3$, $\rho_{Al} = 2707$ kg/m^3 and for the zirconia $E_{Zr} = 151$ GPa, $v_{Zr} = 0.3$, $\rho_{Zr} = 3000$ kg/m^3. These two materials do not have piezo-electro-magnetic properties but the comparison is useful to verify the validity of the code. The considered mechanical load follows a sinusoidal distribution and is defined by introducing a load parameter $P = q_0 a^4 / E_{Zr} h^4$ and the result is provided in dimensionless form $\bar{w} = w/h$. The plate is squared with sides $a = b = 0.2$ m, $h = 0.01$ m and the variation of material properties along the thickness is adjusted by the following relation

$$P(z) = (P_t - P_b)\left(\frac{z}{h} + \frac{1}{2}\right)^{n_p} + P_b, \tag{28}$$

where P_t and P_b indicate top and bottom plate properties, respectively.
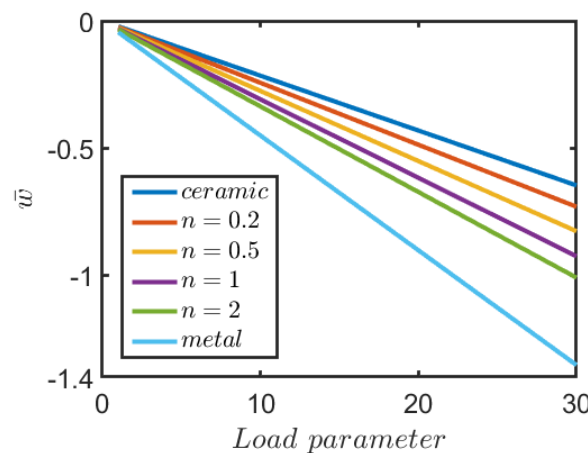
Figure 2. Displacement $\bar{w}$ of middle point of a FG square plate composed of Al/ZrO$_2$ for different values of n_p.

By comparing Figure 2 with the same provided in [74] the results are in very good agreement.

In all the problems that will follow the material properties will be those reported in the Table 1 where the two materials have piezo-electro-magnetic properties. The plate is considered with $a = 1$ m and b is variable according to the problem analyzed. The plate aspect ratio is kept constant as $a/h = 100$. For each application details on the loads applied will be given. The values of the displacement, electrical and magnetic potentials are referred to the central point of the plate and the displacements are reported in dimensionless form according to $\bar{w} = w/h$. In the following, the effects on the behavior of the plate when the nonlocal parameter varies are analyzed. Due to limitations in finding hygro-electro-magnetic properties of materials, the following applications will focus on thermal effects only. Nevertheless, the present model is able to deal with hygroscopic loads also.

Table 1. Piezo-electro-magnetic-thermal properties of materials BaTiO$_3$ and CoFe$_2$O$_4$.

		BaTiO$_3$	**CoFe$_2$O$_4$**
C_{11}	[GPa]	166	286
C_{22}		166	286
C_{33}		162	269.5
C_{13}		78	170.5
C_{23}		78	170.5
C_{12}		77	173
C_{44}		43	45.3
C_{55}		43	45.3
C_{66}		44.5	56.5

Table 1. *Cont.*

		BaTiO$_3$	CoFe$_2$O$_4$
e_{31}	[C/m^2]	-4.4	0
e_{32}		-4.4	0
e_{33}		18.6	0
q_{31}	[N/A·m]	0	580.3
q_{32}		0	580.3
q_{33}		0	699.7
ξ_{11}	[10^{-9}C^2/N·m^2]	11.2	0.08
ξ_{22}		11.2	0.08
ξ_{33}		12.6	0.093
$\zeta_{11} = \zeta_{22} = \zeta_{33}$	[s/m]	0	0
χ_{11}	[10^{-6}N·s^2/C]	5	-590
χ_{22}		5	-590
χ_{33}		10	157
$p_{11} = p_{22}$	[10^{-7} C/m^2 K]	0	0
p_{33}		-11.4	0
$\lambda_{11} = \lambda_{22}$	[10^{-5} Wb/m^2 K]	0	0
λ_{33}		0	-36.2
$\alpha_1 = \alpha_2$	[10^{-6}K^{-1}]	15.8	10
ρ	[kg/m^3]	5300	5800

4.1. Sinusoidal Load

As first application, a square FG plate of width $a = 1$ m and aspect ratio $a/h = 100$ is considered. The plate is subjected to a mechanical load only distributed according to single sinusoidal functions (SDL), therefore the resulting solution is analytical. In the following, Table 2 reports the values of the displacement $\bar{w}$, the electrical potential ϕ and the magnetic potential γ, by varying the FG exponent n_p and the nonlocal parameter ℓ. Since the plate stiffness is increased by the nonlocal parameter, the transverse displacement reduces and the plate is working as a sensor, consequently, electric and magnetic potential reduce with the transverse displacement.

Table 2. Displacement $\bar{w}$, electric and magnetic potential ϕ and γ, of a square nanoplate in central point $(a/2, b/2)$ for different values of nonlocal parameter $(\ell/a)^2$ and n_p (SDL; $q = 10^3$N/m^2, $T_0 = T_1 = 0$ K, $\rho_E = 0$ C/m^2, $\rho_H = 0$ Wb/m^2).

n_p	$(\ell/a)^2$	$\bar{w}$	ϕ [V]	γ [A]
1	0	0.01994	-7.1675	0.6580
	0.05	0.01004	-3.5647	0.3349
	0.10	0.00671	-2.3721	0.2246
0.5	0	0.02067	-11.463	0.4636
	0.05	0.01040	-5.7348	0.2359
	0.10	0.00695	-3.8236	0.1582
2	0	0.01929	-4.7860	0.8932
	0.05	0.00971	-2.3734	0.4531
	0.10	0.00649	-1.5779	0.3036

In Figure 3, the graphs of the vertical displacement and potentials of the BaTiO$_3$/CoFe$_2$O$_4$ plate are presented as the ratio between the edges (a is kept constant) varies and for different values of the nonlocal parameter. The plates are subjected only to a transverse load

$q = 10^3 \text{N/m}^2$. The displacements reduce as in the aforementioned cases due to an increase of the nonlocal parameter, consequently, electric and magnetic potentials are also reduced.

(a)   **(b)**   **(c)**
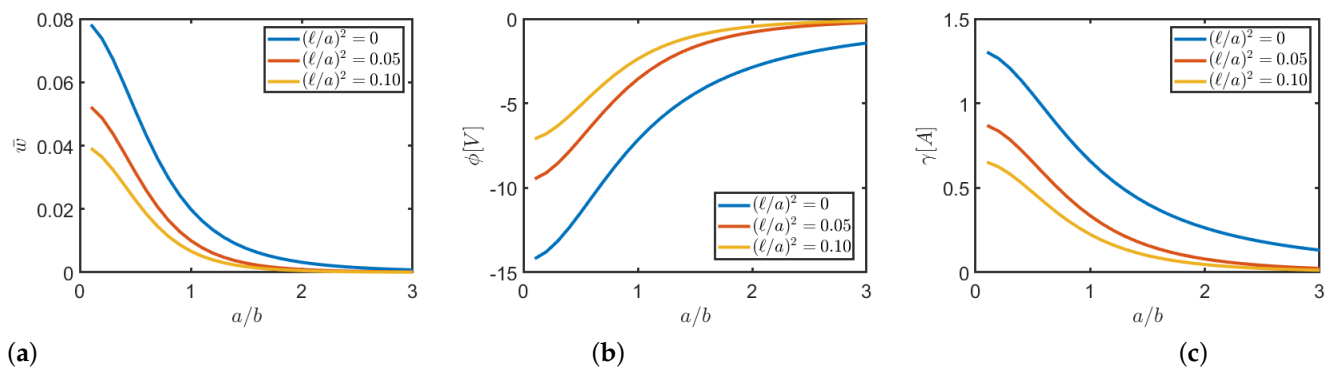
Figure 3. Graphs of displacement $\bar{w}$ (**a**) electric ϕ (**b**) and magnetic γ (**c**) potential, in the point $(a/2, b/2)$ to vary of a/b ratio and for different values of nonlocal parameter $(\ell/a)^2$ and for $n_p = 1$ (SDL; $q = 10^3 \text{ N/m}^2$, $T_0 = T_1 = 0 \text{ K}$, $\rho_E = 0 \text{ C/m}^2$, $\rho_H = 0 \text{ Wb/m}^2$).

Tables 3–5 list the values of the displacement $\bar{w}$, the electric potential ϕ and the magnetic potential γ, due to the sinusoidally distributed (SDL) action of a thermal load that varies linearly along the thickness, an electric charge density and a magnetic charge density on the plate surface. It is noted that with respect to the mechanical load a relatively small temperature rise of $T_1 = 1 \text{ K}$ leads to higher electric and magnetic fields and smaller mechanical deflections. In addition, it is obvious that by applying electric or magnetic densities the correspondent fields are of several orders of magnitude higher than the other mechanical and thermal loads.

Table 3. Displacement $\bar{w}$, electric and magnetic potential ϕ and γ, of a square nanoplate in central point $(a/2, b/2)$ for different values of nonlocal parameter $(\ell/a)^2$ and n_p. (SDL; $q = 0 \text{ N/m}^2$, $T_0 = 0 \text{ K}$, $T_1 = 1 \text{ K}$, $\rho_E = 0 \text{ C/m}^2$, $\rho_H = 0 \text{ Wb/m}^2$).

n_p	$(\ell/a)^2$	$\bar{w}$	ϕ [V]	γ [A]
1	0	0.00855	−3.4621	0.2359
	0.05	0.00430	−1.7194	0.1208
	0.10	0.00287	−1.1435	0.0812
0.5	0	0.00898	−5.4569	0.1739
	0.05	0.00452	−2.7300	0.0888
	0.10	0.00302	−1.8201	0.0595
2	0	0.00819	−2.3699	0.3132
	0.05	0.00412	−1.1716	0.1598
	0.10	0.00275	−0.7781	0.1073

Table 4. Displacement $\bar{w}$, electric and magnetic potential ϕ and γ, of a square nanoplate in central point $(a/2, b/2)$ for different values of nonlocal parameter $(\ell/a)^2$ and n_p. (SDL; $q = 0$ N/m^2, $T_0 = T_1 = 0$ K, $\rho_E = 0.1$ C/m^2, $\rho_H = 0$ Wb/m^2).

n_p	$(\ell/a)^2$	$\bar{w}$	ϕ [10^3 V]	γ [A]
1	0	−0.07168	−3.7535	4.6774
	0.05	−0.03565	−1.8899	2.2793
	0.10	−0.02372	−1.2626	1.5288
0.5	0	−0.11463	−4.6931	5.6947
	0.05	−0.05735	−2.3627	2.8018
	0.10	−0.03824	−1.5786	1.8745
2	0	−0.04786	−3.2178	4.2379
	0.05	−0.02373	−1.6199	2.0733
	0.10	−0.01578	−1.0823	1.3924

Table 5. Displacement $\bar{w}$, electric and magnetic potential ϕ and γ, of a square nanoplate in central point $(a/2, b/2)$ for different values of nonlocal parameter $(\ell/a)^2$ and n_p. (SDL; $q = 0$ N/m^2, $T_0 = T_1 = 0$ K, $\rho_E = 0$ C/m^2, $\rho_H = 1$ Wb/m^2).

n_p	$(\ell/a)^2$	$\bar{w}$	ϕ [10 V]	γ [10^2 A]
1	0	0.06580	4.6773	−3.4533
	0.05	0.03349	2.2793	−1.7383
	0.10	0.02246	1.5288	−1.1612
0.5	0	0.04636	5.6947	−2.9196
	0.05	0.02359	2.8018	−1.4696
	0.10	0.01582	1.8744	−0.9818
2	0	0.08932	4.2379	−4.0778
	0.05	0.04531	2.0733	−2.0525
	0.10	0.03036	1.3924	−1.3712

Figures 4 and 5 report the the middle point displacements, electric and magnetic potential, as a function of the a/b ratio and for different values of the nonlocal parameter. Load data are reported in each figure caption. In all cases the nonlocal effect plays a relevant role in the evaluation of the electric and potential fields when loads different to the mechanical one are applied. In fact, a negligible variation is observed for $(\ell/a)^2 = 0$ on the contrary evident variations are visible for the other cases as b decreases (a/b increases). This phenomenon is not reflected in the transverse displacement which behaves closely in the same way both for the local and nonlocal cases.

Finally, Figure 6 shows the displacements, electric and magnetic potentials of the central point of the plate subjected to a SDL magnetic charge density. From graph Figure 6a it can be seen that for $n_p = 0$ the displacement is null as the material is purely piezo-electric, while for $n_p > 0$ the displacements increase as the composition of the plate becomes piezo-magnetic.
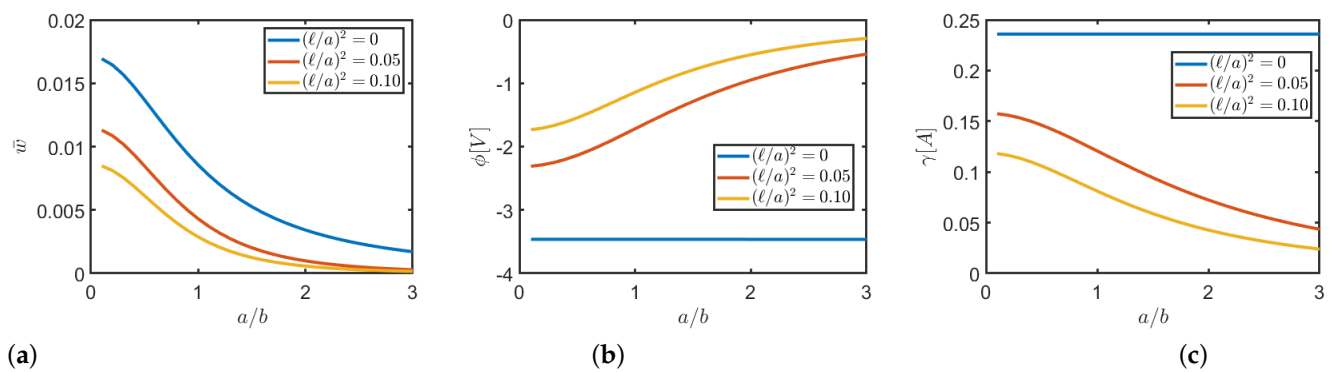
Figure 4. Graphs of displacement $\bar{w}$ (**a**) electric ϕ (**b**) and magnetic γ (**c**) potential, in the point $(a/2, b/2)$ to vary of a/b ratio and for different values of nonlocal parameter $(\ell/a)^2$ and for $n_p = 1$. (SDL; $q = 0$ N/m^2, $T_0 = 0$ K, $T_1 = 1$ K, $\rho_E = 0$ C/m^2, $\rho_H = 0$ Wb/m^2)
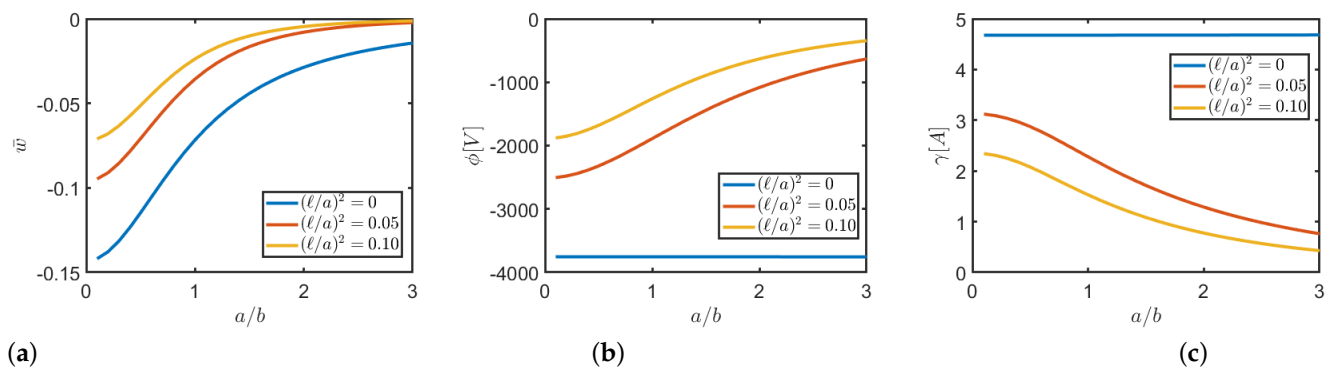
Figure 5. Graphs of displacement $\bar{w}$ (**a**) electric ϕ (**b**) and magnetic γ (**c**) potential, in the point $(a/2, b/2)$ to vary of a/b ratio and for different values of nonlocal parameter $(\ell/a)^2$ and for $n_p = 1$. (SDL; $q = 0$ N/m^2, $T_0 = T_1 = 0$ K, $\rho_E = 0.1$ C/m^2, $\rho_H = 0$ Wb/m^2)
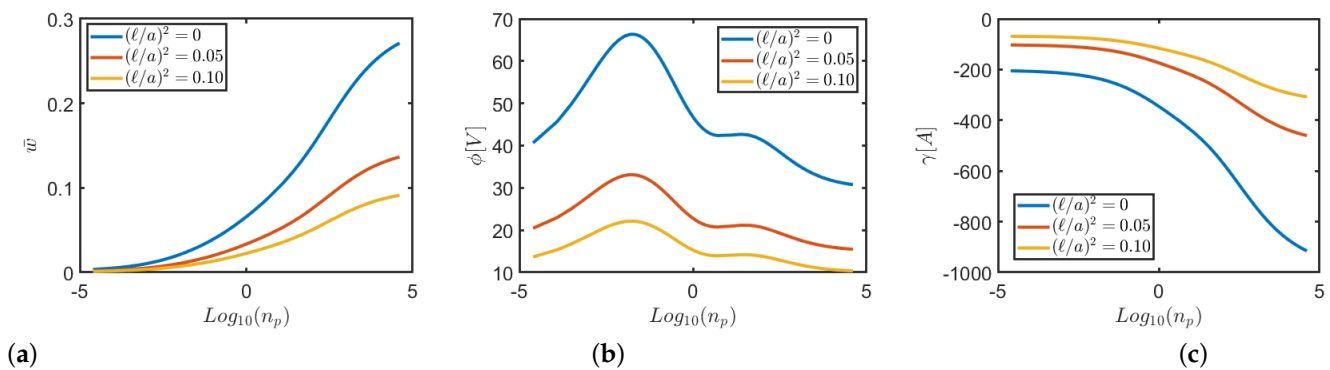
Figure 6. Graphs of displacement $\bar{w}$ (a) electric ϕ (b) and magnetic γ (c) potential, in the point $(a/2, b/2)$ to vary of n_p and for different values of nonlocal parameter $(\ell/a)^2$ and for $n_p = 1$. (SDL; $q = 0$ N/m^2, $T_0 = T_1 = 0$ K, $\rho_E = 0$ C/m^2, $\rho_H = 1$ Wb/m^2)

4.2. Uniform Load

Unlike the sinusoidal case which leads to an exact solution for the present problem, the uniform load gives an approximate solution and its accuracy depends on the expansion order selected. Therefore, before discussing the results obtained with uniform loading a convergence analysis is performed. Figure 7a shows the convergence of the transverse displacement as well as the electric potential by increasing the expansion order (m, n). The convergence is computed in terms of relative error with respect to the value obtained for $(m, n) = 299$. It is clear that two convergence trends take place and the displacements show a faster accuracy with respect to the potential. From the graph it can be deduced that $(m, n) = 199$ is already a sufficient number of semi-waves to accurately approximate the

displacements within a reasonable error, whereas for the electrical and magnetic potentials the error is larger but still small for engineering applications. It is specified that in Figure 7a is reported only the electrical potential because the error curves is equal to the one obtained for the magnetic potential. As for the cases just discussed for SDL, tables and graphs are reported for each type of uniform applied load (UDL).

As for the mechanical load, convergence test is performed also for the uniformly distributed thermal load by checking transverse displacement and electric potential as in the case above. Figure 7b shows that the error made on both displacement and potential is several orders of magnitude larger than in the case of uniform mechanical loading, where the displacement looks more accurate as in the previous case.

(a)　　**(b)**
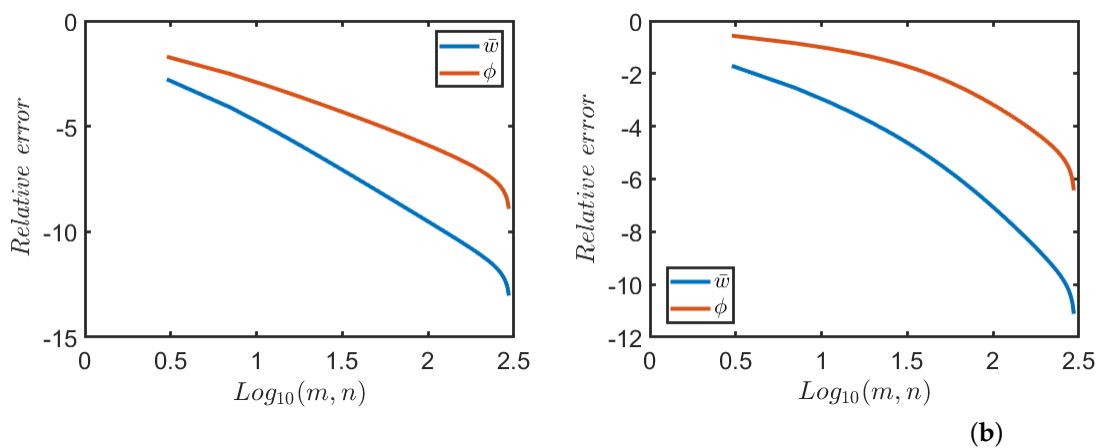
Figure 7. Convergence of the relative error on the displacement and potential at a square plate central point by increasing (m, n) for: (**a**) uniformly distributed mechanical load only; (**b**) uniformly distributed thermal load only.

Considering both convergence trends, an expansion with $(m, n) = 199$ is considered in the following computations. Therefore, the results listed and shown below will be accurate up to the accuracy levels indicated in Figure 7.

The results in terms of maximum displacement and electric and magnetic potentials are listed in Table 6 by varying the FG exponent and the nonlocal parameter. The plate under consideration is squared $a = b$ and the plate is subjected to UDL mechanical load. As for the SDL, displacements and potentials decrease by increasing the nonlocal parameter. In addition the magnetic potential changes sign for a FG distribution $n_p = 2$. A graphical representation of the displacement and potentials variations according to a/b and nonlocal parameter variation is depicted in Figure 8. The plots are presented for $n_p = 1$ and the potentials decrease as well as the transverse displacement by increasing a/b with a constant.

Table 6. Displacement $\bar{w}$, electric and magnetic potential ϕ and γ, of a square nanoplate in central point $(a/2, b/2)$ for different values of nonlocal parameter $(\ell/a)^2$ and n_p (UDL; $q = 10^3$ N/m², $T_0 = T_1 = 0$ K, $\rho_E = 0$ C/m², $\rho_H = 0$ Wb/m²).

n_p	$(\ell/a)^2$	$\bar{w}$	ϕ [V]	γ [A]
1	0	0.03156	-10.413	0.9571
	0.05	0.01614	-5.5579	0.5214
	0.10	0.01080	-3.7245	0.3523
0.5	0	0.03271	-16.668	0.6744
	0.05	0.01672	-8.9377	0.3672
	0.10	0.01119	-6.0017	0.2481
2	0	0.03054	-6.9616	1.2988
	0.05	0.01561	-3.7011	0.7055
	0.10	0.01044	-2.4779	0.4761

(a)   **(b)**   **(c)**
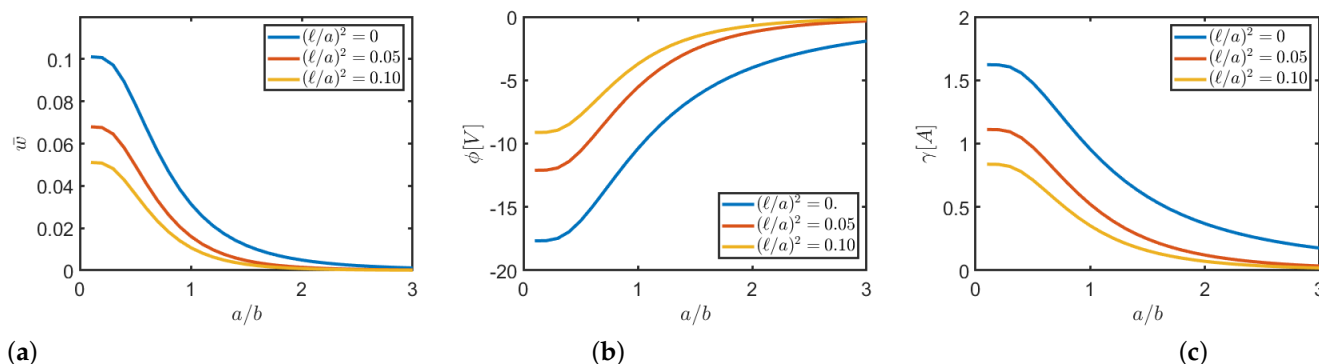
Figure 8. Displacement $\bar{w}$ (**a**) electric ϕ (**b**) and magnetic γ (**c**) potential, at the central point $(a/2, b/2)$ by varying a/b and for different nonlocal parameters $(\ell/a)^2$ with $n_p = 1$ (UDL; $q = 10^3 \mathrm{N/m^2}$, $T_0 = T_1 = 0$ K, $\rho_E = 0\,\mathrm{C/m^2}$, $\rho_H = 0\,\mathrm{Wb/m^2}$).

In Table 7, the results obtained for a square plate FG subjected to a UDL thermal load on the surface and variable linearly along the thickness are reported.

Table 7. Displacement $\bar{w}$, electric and magnetic potential ϕ and γ, of a square nanoplate at the central point $(a/2, b/2)$ for different values of nonlocal parameter $(\ell/a)^2$ and n_p (UDL; $q = 0\mathrm{N/m^2}$, $T_0 = 0$, $T_1 = 1$ K, $\rho_E = 0\,\mathrm{C/m^2}$, $\rho_H = 0\,\mathrm{Wb/m^2}$).

n_p	$(\ell/a)^2$	$\bar{w}$	ϕ [V]	γ [A]
1	0	0.01243	−3.4601	0.2357
	0.05	0.00670	−2.3305	0.1620
	0.10	0.00451	−1.6021	0.1128
0.5	0	0.01306	−5.4536	0.1738
	0.05	0.00704	−3.6912	0.1192
	0.10	0.00474	−2.5452	0.0829
2	0	0.01191	−2.3686	0.3129
	0.05	0.00642	−1.5904	0.2146
	0.10	0.00432	−1.0914	0.1492

Figure 9 shows the results obtained for the same type of load described in Table 7, by varying the plate ratio a/b and for $n_p = 1$. Negligible variations are observed for the potentials with $(\ell/a)^2 = 0$ as occurred in the SDL case.

(a)   **(b)**   **(c)**
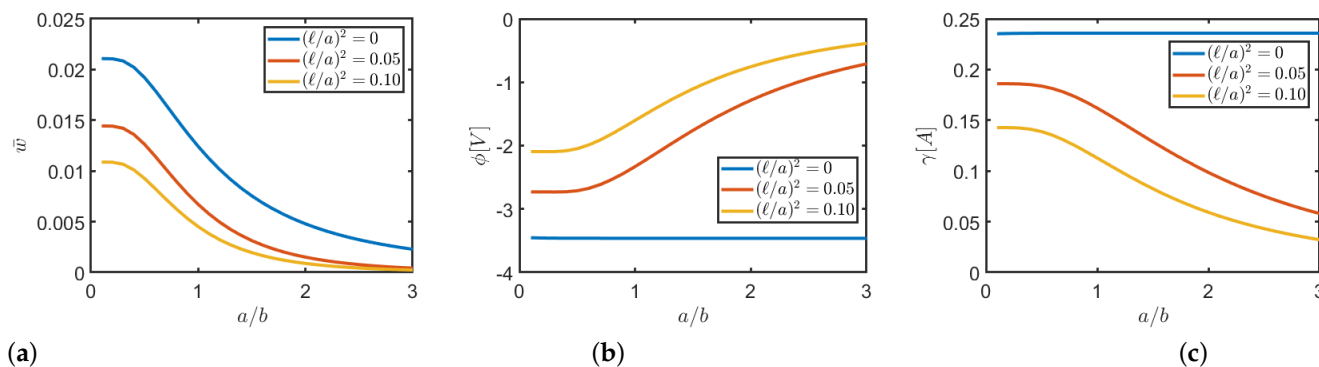
Figure 9. Displacement $\bar{w}$ (**a**) electric ϕ (**b**) and magnetic γ (**c**) potential, at the central point $(a/2, b/2)$ by varying a/b ratio and for different nonlocal parameter $(\ell/a)^2$ with $n_p = 1$ (UDL; $q = 0\,\mathrm{N/m^2}$, $T_0 = 0$ K, $T_1 = 1$ K, $\rho_E = 0\,\mathrm{C/m^2}$, $\rho_H = 0\,\mathrm{Wb/m^2}$).

In Tables 8 and 9 the results obtained for a square FG plate are reported, for different types of load applied with the common characteristic of being uniformly distributed on the surface. Load values are reported in the table captions. Coupling effects in terms of

sensing/actuating actions are observed when electric and magnetic densities are applied as expected. With respect to all the other cases presented, Table 9 with $n_p = 2$ presents an opposite elastic deformation of the plate when magnetic density is applied.

Table 8. Displacement $\bar{w}$, electric and magnetic potential ϕ and γ, of a square nanoplate in central point $(a/2, b/2)$ for different values of nonlocal parameter $(\ell/a)^2$ and n_p (UDL; $q = 0$ N/m^2, $T_0 = T_1 = 0$ K, $\rho_E = 0.1$ C/m^2, $\rho_H = 0$ Wb/m^2).

n_p	$(\ell/a)^2$	$\bar{w}$	ϕ [10^3 V]	γ [A]
1	0	-0.10421	-3.7513	4.6753
	0.05	-0.05558	-2.5500	3.0680
	0.10	-0.03725	-1.7627	2.1258
0.5	0	-0.16647	-4.6922	5.6941
	0.05	-0.08938	-3.1879	3.7784
	0.10	-0.06002	-2.2038	2.6124
2	0	-0.06950	-3.2171	4.2377
	0.05	-0.03701	-2.1859	2.7877
	0.10	-0.02478	-1.5110	1.9346

Table 9. Displacement $\bar{w}$, electric and magnetic potential ϕ and γ, of a square nanoplate in central point $(a/2, b/2)$ for different values of nonlocal parameter $(\ell/a)^2$ and n_p. (UDL; $q = 0$ N/m^2, $T_0 = T_1 = 0$ K, $\rho_E = 0$ C/m^2, $\rho_H = 1$ Wb/m^2).

n_p	$(\ell/a)^2$	$\bar{w}$	ϕ [10 V]	γ [10^2 A]
1	0	0.09568	4.6753	-3.4507
	0.05	0.05214	3.0680	-2.3456
	0.10	0.03523	2.1258	-1.6213
0.5	0	0.06733	5.6941	-2.9191
	0.05	0.03672	3.7784	-1.9830
	0.10	0.02481	2.6124	-1.3707
2	0	0.12971	4.2377	-4.0772
	0.05	0.07055	2.7877	-2.7697
	0.10	0.04761	1.9346	-1.9144

Graphical representation of the same configurations are displayed in Figures 10 and 11 as a function of the a/b ratio and the nonlocal parameter with $n_p = 1$. From these graphs it is possible to observe how for the uniform distribution, as already detected for the sinusoidal distribution, except in the case of mechanical load, the potentials are almost invariant with respect to the a/b ratio for the null value of the nonlocal parameter. For the present value of the FG parameter as shown also in the correspondent Table 8 electric and magnetic potentials have opposite signs, thus on one hand the plate works as a sensor and on the other hand as an actuator.
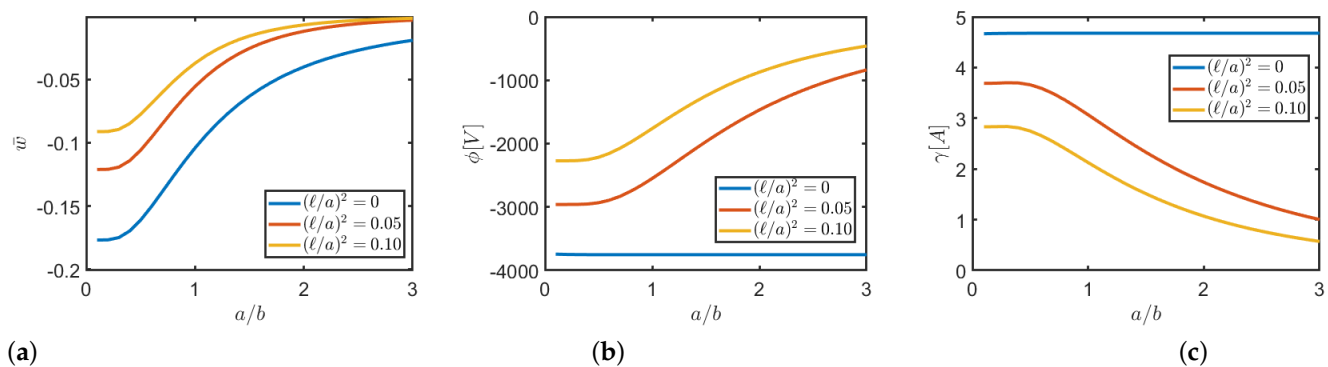
Figure 10. Graphs of displacement $\bar{w}$ (**a**) electric ϕ (**b**) and magnetic γ (**c**) potential, in the point $(a/2, b/2)$ to vary of a/b ratio and for different values of nonlocal parameter $(\ell/a)^2$ and for $n_p = 1$. (UDL; $q = 0$ N/m^2, $T_0 = T_1 = 0$ K, $\rho_E = 0.1$ C/m^2, $\rho_H = 0$ Wb/m^2).
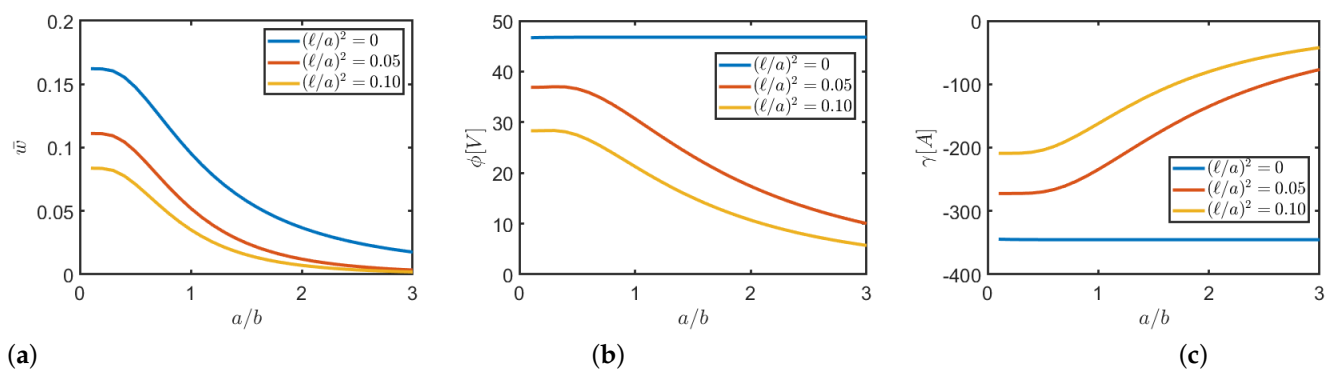
Figure 11. Graphs of displacement $\bar{w}$ (**a**) electric ϕ (**b**) and magnetic γ (**c**) potential, in the point $(a/2, b/2)$ to vary of a/b ratio and for different values of nonlocal parameter $(\ell/a)^2$ and for $n_p = 1$. (UDL; $q = 0$ N/m^2, $T_0 = T_1 = 0$ K, $\rho_E = 0$ C/m^2, $\rho_H = 1$ Wb/m^2).

5. Conclusions

The focus of this paper was to investigate the effects of the nonlocal parameter on the bending analysis of functionally graded magneto-electro-thermo-elastic nanoplates subjected to different types of load in hygro-thermal environment. The equilibrium equations are carried out via the principle of virtual work and solved by using the trigonometric framework of Navier approach. The materials that have been used in the simulations are BaTiO$_3$ and CoFe$_2$O$_4$ and the properties of the materials used are reported in the article according to a classical FG power law. Tables and graphs show the results obtained for mechanical, electrical, magnetic and thermal loads, distributed sinusoidally and uniformly on the plate middle surface. For uniform loads, convergence analyses of the results are also reported, which allowed the identification of the appropriate number of half-waves needed to best approximate the distribution of the parameters. The results show a decrease in displacements as the nonlocal parameter increases for all loading conditions. A decrease in absolute values is also observed for potentials as the nonlocal parameter increases, but positive or negative values of electric and magnetic potentials are observed alternatively as a function of the applied electric and magnetic densities. Furthermore, from the graphs, it is evident that for both sinusoidal and uniform loads, the aspect ratio has little influence on the value of the potentials, with a negligible value of the nonlocal parameter.

Author Contributions: Conceptualization, N.F.; methodology, N.F.; software, N.F. and G.T.M.; validation, N.F. and G.T.M.; formal analysis, N.F. and G.T.M.; investigation, N.F. and G.T.M.; resources, N.F., F.F. and R.L.; data curation, G.T.M.; writing—original draft preparation, N.F. and G.T.M.; writing—review and editing, N.F., G.T.M., F.F. and R.L.; visualization, F.F. and R.L.; supervision, N.F., F.F. and R.L.; project administration, N.F., F.F. and R.L.; funding acquisition, F.F. and R.L. All authors have read and agreed to the published version of the manuscript.

Appendix A

Integrating along thickness thermal properties $\mathbf{Q}(z)\boldsymbol{\alpha}(z)$ and hygrometric properties $\mathbf{Q}(z)\boldsymbol{\beta}(z)$, it is obtained:

$$\mathbf{A}^{\alpha} = \int_{-\frac{h}{2}}^{\frac{h}{2}} \mathbf{Q}(z)\boldsymbol{\alpha}(z)\,dz, \quad \mathbf{B}^{\alpha} = \int_{-\frac{h}{2}}^{\frac{h}{2}} \mathbf{Q}(z)\boldsymbol{\alpha}(z)z\,dz, \quad \mathbf{D}^{\alpha} = \int_{-\frac{h}{2}}^{\frac{h}{2}} \mathbf{Q}(z)\boldsymbol{\alpha}(z)z^2\,dz \quad \text{(A1)}$$

$$\mathbf{A}^{\beta} = \int_{-\frac{h}{2}}^{\frac{h}{2}} \mathbf{Q}(z)\boldsymbol{\beta}(z)dz, \quad \mathbf{B}^{\beta} = \int_{-\frac{h}{2}}^{\frac{h}{2}} \mathbf{Q}(z)\boldsymbol{\beta}(z)zdz, \quad \mathbf{D}^{\beta} = \int_{-\frac{h}{2}}^{\frac{h}{2}} \mathbf{Q}(z)\boldsymbol{\beta}(z)z^2dz \quad \text{(A2)}$$

Integrating last two integrals of Equation (15) along the thickness the following quantities can be defined:

$$
\begin{aligned}
\mathbf{A}_E^f &= \int_{-\frac{h}{2}}^{\frac{h}{2}} \tilde{\mathbf{e}}\mathbf{f}_E\,dz, \quad \mathbf{A}_E = \int_{-\frac{h}{2}}^{\frac{h}{2}} \tilde{\mathbf{e}}\,dz, \quad \mathbf{B}_E^f = \int_{-\frac{h}{2}}^{\frac{h}{2}} \tilde{\mathbf{e}}\mathbf{f}_E\,z\,dz \quad, \quad \mathbf{B}_E = \int_{-\frac{h}{2}}^{\frac{h}{2}} \tilde{\mathbf{e}}\,z\,dz \\
\mathbf{A}_H^f &= \int_{-\frac{h}{2}}^{\frac{h}{2}} \tilde{\mathbf{q}}\mathbf{f}_H\,dz, \quad \mathbf{A}_H = \int_{-\frac{h}{2}}^{\frac{h}{2}} \tilde{\mathbf{q}}\,dz, \quad \mathbf{B}_H^f = \int_{-\frac{h}{2}}^{\frac{h}{2}} \tilde{\mathbf{q}}\mathbf{f}_H\,z\,dz, \quad \mathbf{B}_H = \int_{-\frac{h}{2}}^{\frac{h}{2}} \tilde{\mathbf{q}}\,z\,dz
\end{aligned} \quad \text{(A3)}
$$

$$
\begin{aligned}
\mathbf{A}_{\zeta}^f &= \int_{-\frac{h}{2}}^{\frac{h}{2}} \mathbf{f}_E^{\top}\tilde{\boldsymbol{\xi}}dz, \quad \mathbf{B}_{\zeta}^f = \int_{-\frac{h}{2}}^{\frac{h}{2}} \mathbf{f}_E^{\top}\tilde{\boldsymbol{\xi}}\mathbf{f}_Edz, \quad \mathbf{A}_{\zeta} = \int_{-\frac{h}{2}}^{\frac{h}{2}} \mathbf{f}_E^{\top}\tilde{\boldsymbol{\zeta}}dz, \quad \mathbf{B}_{\zeta} = \int_{-\frac{h}{2}}^{\frac{h}{2}} \mathbf{f}_E^{\top}\tilde{\boldsymbol{\zeta}}\mathbf{f}_Hdz \\
\mathbf{A}_p &= \int_{-\frac{h}{2}}^{\frac{h}{2}} \mathbf{f}_E^{\top}\mathbf{p}dz, \quad \mathbf{B}_p = \int_{-\frac{h}{2}}^{\frac{h}{2}} \mathbf{f}_E^{\top}\mathbf{p}z\,dz, \quad \mathbf{A}_h = \int_{-\frac{h}{2}}^{\frac{h}{2}} \mathbf{f}_E^{\top}\mathbf{h}dz, \quad \mathbf{B}_h = \int_{-\frac{h}{2}}^{\frac{h}{2}} \mathbf{f}_E^{\top}\mathbf{h}z\,dz
\end{aligned} \quad \text{(A4)}
$$

$$
\begin{aligned}
\mathbf{A}_{\zeta}^f &= \int_{-\frac{h}{2}}^{\frac{h}{2}} \mathbf{f}_H^{\top}\tilde{\boldsymbol{\zeta}}dz, \quad \mathbf{B}_{\zeta}^f = \int_{-\frac{h}{2}}^{\frac{h}{2}} \mathbf{f}_H^{\top}\tilde{\boldsymbol{\zeta}}\mathbf{f}_Edz, \quad \mathbf{A}_{\chi}^f = \int_{-\frac{h}{2}}^{\frac{h}{2}} \mathbf{f}_H^{\top}\tilde{\boldsymbol{\chi}}dz, \quad \mathbf{B}_{\chi}^f = \int_{-\frac{h}{2}}^{\frac{h}{2}} \mathbf{f}_H^{\top}\tilde{\boldsymbol{\chi}}\mathbf{f}_Hdz \\
\mathbf{A}_{\lambda} &= \int_{-\frac{h}{2}}^{\frac{h}{2}} \mathbf{f}_H^{\top}\boldsymbol{\lambda}dz, \quad \mathbf{B}_{\lambda} = \int_{-\frac{h}{2}}^{\frac{h}{2}} \mathbf{f}_H^{\top}\boldsymbol{\lambda}z\,dz, \quad \mathbf{A}_{\eta} = \int_{-\frac{h}{2}}^{\frac{h}{2}} \mathbf{f}_H^{\top}\boldsymbol{\eta}dz, \quad \mathbf{B}_{\eta} = \int_{-\frac{h}{2}}^{\frac{h}{2}} \mathbf{f}_H^{\top}\boldsymbol{\eta}z\,dz
\end{aligned} \quad \text{(A5)}
$$

Considering what reported in Equations (A3)–(A5) the coefficients $\hat{c}_{ij}$, for $i,j = 1, 2, \ldots, 5$ can be written as

$$
\begin{aligned}
\hat{c}_{11} &= \alpha^2 A_{11} + \beta^2 A_{66} + \ell^2 \left[\alpha^4 A_{11} + \alpha^2\beta^2(A_{11} + A_{66}) + \beta^4 A_{66}\right] \\
\hat{c}_{12} &= \alpha\beta(A_{12} + A_{66}) + \ell^2 \left[\alpha^3\beta(A_{12} + A_{66}) + \alpha\beta^3(A_{12} + A_{66})\right] \\
\hat{c}_{13} &= -\alpha^3 B_{11} - \alpha\beta^2(B_{12} + 2B_{66}) \\
&\quad - \ell^2 \left[\alpha^5 B_{11} + \alpha^3\beta^2(B_{12} + B_{11} + 2B_{66}) + \alpha\beta^4(B_{12} + 2B_{66})\right] \\
\hat{c}_{14} &= -\alpha A_{E,13}^f + \ell^2 \left[-\alpha^3 A_{E,13}^f - \alpha\beta^2 A_{E,13}^f\right] \\
\hat{c}_{15} &= -\alpha A_{H,13}^f + \ell^2 \left[-\alpha^3 A_{H,13}^f - \alpha\beta^2 A_{H,13}^f\right]
\end{aligned} \quad \text{(A6)}
$$

$$\hat{c}_{22} = \beta^2 A_{22} + \alpha^2 A_{66} + \ell^2 \left[\alpha^2 \beta^2 (A_{22} + A_{66}) + \alpha^4 A_{66} + \beta^4 A_{22} \right]$$

$$\hat{c}_{23} = -\alpha^2 \beta (B_{12} + 2B_{66}) - \beta^3 B_{22}$$
$$- \ell^2 \left[\alpha^4 \beta (B_{12} + 2B_{66}) + \alpha^2 \beta^3 (B_{22} + B_{12} + 2B_{66}) + \beta^5 B_{22} \right] \tag{A7}$$

$$\hat{c}_{24} = \beta A^f_{E,23} - \ell^2 \left[-\beta^3 A^f_{E,23} - \alpha^2 \beta A^f_{E,23} \right]$$

$$\hat{c}_{25} = \beta A^f_{H,23} - \ell^2 \left[-\beta^3 A^f_{H,23} - \alpha^2 \beta A^f_{H,23} \right]$$

$$\hat{c}_{33} = \alpha^4 D_{11} + 2\alpha^2 \beta^2 (D_{12} + 2D_{66}) + \beta^4 D_{22} + \ell^2 \left[\alpha^6 D_{11} + \alpha^4 \beta^2 (D_{11} + 2D_{12} + 4D_{66}) \right.$$
$$\left. + \alpha^2 \beta^4 (D_{22} + 2D_{12} + 4D_{66}) + \beta^6 D_{22} \right] \tag{A8}$$

$$\hat{c}_{34} = \alpha^2 B^f_{E,13} + \beta^2 B^f_{E,23} + \ell^2 \left[\alpha^4 B^f_{E,13} + \alpha^2 \beta^2 \left(B^f_{E,13} + B^f_{E,23} \right) + \beta^4 B^f_{E,23} \right]$$

$$\hat{c}_{35} = \alpha^2 B^f_{H,13} + \beta^2 B^f_{H,23} + \ell^2 \left[\alpha^4 B^f_{H,13} + \alpha^2 \beta^2 \left(B^f_{H,13} + B^f_{H,23} \right) + \beta^4 B^f_{H,23} \right]$$

$$\hat{c}_{44} = -B^f_{\xi,33} - \alpha^2 B^f_{\xi,11} - \beta^2 B^f_{\xi,22}$$
$$- \ell^2 \left[\alpha^4 B^f_{\xi,11} + \alpha^2 \beta^2 \left(B^f_{\xi,11} + B^f_{\xi,22} \right) + \beta^4 B^f_{\xi,22} + \alpha^2 B^f_{\xi,33} + \beta^2 B^f_{\xi,33} \right]$$

$$\hat{c}_{45} = -B^{fE}_{\zeta,33} - \alpha^2 B^{fE}_{\zeta,11} - \beta^2 B^{fE}_{\zeta,22}$$
$$- \ell^2 \left[\alpha^4 B^{fE}_{\zeta,11} + \alpha^2 \beta^2 \left(B^{fE}_{\zeta,11} + B^{fE}_{\zeta22} \right) + \beta^4 B^{fE}_{\zeta,22} + \alpha^2 B^{fE}_{\zeta,33} + \beta^2 B^{fE}_{\zeta,33} \right]$$

$$\hat{c}_{54} = -B^{fH}_{\zeta,33} - \alpha^2 B^{fH}_{\zeta,11} - \beta^2 B^{fH}_{\zeta,22} \tag{A9}$$
$$- \ell^2 \left[\alpha^4 B^{fH}_{\zeta,11} + \alpha^2 \beta^2 \left(B^{fH}_{\zeta,11} + B^{fH}_{\zeta,22} \right) + \beta^4 B^{fH}_{\zeta,22} + \alpha^2 B^{fH}_{\zeta,33} + \beta^2 B^{fH}_{\zeta,33} \right]$$

$$\hat{c}_{55} = -B^f_{\chi,33} - \alpha^2 B^f_{\chi,11} - \beta^2 B^f_{\chi22}$$
$$- \ell^2 \left[\alpha^4 B^f_{\chi,11} + \alpha^2 \beta^2 \left(B^f_{\chi,11} + B^f_{\chi,22} \right) + \beta^4 B^f_{\chi,22} + \alpha^2 B^f_{\chi,33} + \beta^2 B^f_{\chi,33} \right]$$

$$\tilde{s}_{33} = \alpha \left(\hat{N}_{xx} + \hat{N}^T_{xx} + \hat{N}^E_{xx} + \hat{N}^H_{xx} \right) + \beta \left(\hat{N}_{yy} + \hat{N}^T_{yy} + \hat{N}^E_{yy} + \hat{N}^H_{yy} \right)$$

In the present case electric and magnetic potentials have the same expansion through-the-thickness as shown in Equation (9), thus, $\mathbf{B}^{fE}_{\zeta} = \mathbf{B}^{fH}_{\zeta} = \mathbf{B}^f_{\zeta}$, hence, $\hat{c}_{45} = \hat{c}_{54}$.

The vector of hygro-thermal loads turns out to have the following form

$$\mathcal{F}^T_{1,mn} = -\alpha \left[\left(A^\alpha_1 T_{0,mn} + \frac{1}{h} B^\alpha_1 T_{1,mn} \right) + \left(A^\beta_1 C_{0,mn} + \frac{1}{h} B^\beta_1 C_{1,mn} \right) \right]$$

$$\mathcal{F}^T_{2,mn} = -\beta \left[\left(A^\alpha_2 T_{0,mn} + \frac{1}{h} B^\alpha_2 T_{1,mn} \right) + \left(A^\beta_2 C_{0,mn} + \frac{1}{h} B^\beta_2 C_{1,mn} \right) \right]$$

$$\mathcal{F}^T_{3,mn} = \alpha^2 \left[\left(B^\alpha_1 T_{0,mn} + \frac{1}{h} D^\alpha_1 T_{1,mn} \right) + \left(B^\beta_1 C_{0,mn} + \frac{1}{h} D^\beta_1 C_{1,mn} \right) \right] \tag{A10}$$

$$+ \beta^2 \left[\left(B^\alpha_2 T_{0,mn} + \frac{1}{h} D^\alpha_2 T_{1,mn} \right) + \left(B^\beta_2 C_{0,mn} + \frac{1}{h} D^\beta_2 C_{1,mn} \right) \right]$$

$$\mathcal{F}^T_{4,mn} = -A_{p,3} T_{0,mn} - B_{p,3} \frac{1}{h} T_{1,mn} - A_{h,3} C_{0,mn} - B_{h,3} \frac{1}{h} C_{1,mn}$$

$$\mathcal{F}^T_{5,mn} = -A_{\lambda,3} T_{0,mn} - B_{\lambda,3} \frac{1}{h} T_{1,mn} - A_{\eta,3} C_{0,mn} - B_{\eta,3} \frac{1}{h} C_{1,mn}$$

References

1. Berman, D.; Krim, J. Surface science, MEMS and NEMS: Progress and opportunities for surface science research performed on, or by, microdevices. *Prog. Surf. Sci.* **2013**, *88*, 171–211. [CrossRef]
2. Ekinci, K.L.; Roukes, M.L. Nanoelectromechanical systems. *Rev. Sci. Instrum.* **2005**, *76*, 061101. [CrossRef]
3. Bhushan, B. Nanotribology and nanomechanics of MEMS/NEMS and BioMEMS/BioNEMS materials and devices. *Microelectron. Eng.* **2007**, *84*, 387–412. [CrossRef]
4. Chu, Z.; PourhosseiniAsl, M.; Dong, S. Review of multi-layered magnetoelectric composite materials and devices applications. *J. Phys. D Appl. Phys.* **2018**, *51*, 243001. [CrossRef]
5. Bonanni, A.; del Valle, M. Use of nanomaterials for impedimetric DNA sensors: A review. *Anal. Chim. Acta* **2010**, *678*, 7–17. [CrossRef]
6. Morsin, M.; Mat Salleh, M.; Ali Umar, A.; Sahdan, M. Gold Nanoplates for a Localized Surface Plasmon Resonance-Based Boric Acid Sensor. *Sensors* **2017**, *17*, 947. [CrossRef]
7. Wu, W. Inorganic nanomaterials for printed electronics: A review. *Nanoscale* **2017**, *9*, 7342–7372. [CrossRef] [PubMed]
8. Gohardani, O.; Elola, M.C.; Elizetxea, C. Potential and prospective implementation of carbon nanotubes on next generation aircraft and space vehicles: A review of current and expected applications in aerospace sciences. *Prog. Aerosp. Sci.* **2014**, *70*, 42–68. [CrossRef]
9. La, D.; Nguyen, T.; Jones, L.; Bhosale, S. Graphene-Supported Spinel $CuFe_2O_4$ Composites: Novel Adsorbents for Arsenic Removal in Aqueous Media. *Sensors* **2017**, *17*, 1292. [CrossRef]
10. Singh, T. A review of nanomaterials in civil engineering works. *Inter. J. Struct. Civ. Eng. Res.* **2014**, *3*, 31–35.
11. Guo, H.; Yang, T.; Żur, K.K.; Reddy, J. On the flutter of matrix cracked laminated composite plates reinforced with graphene nanoplatelets. *Thin-Walled Struct.* **2021**, *158*, 107161. [CrossRef]
12. Mancusi, G.; Fabbrocino, F.; Feo, L.; Fraternali, F. Size effect and dynamic properties of 2D lattice materials. *Compos. Part B Eng.* **2017**, *112*, 235–242. [CrossRef]
13. Fabbrocino, F.; Carpentieri, G. Three-dimensional modeling of the wave dynamics of tensegrity lattices. *Compos. Struct.* **2017**, *173*, 9–16. [CrossRef]
14. Lakes, R. Experimental microelasticity of two porous solids. *Int. J. Solids Struct.* **1986**, *22*, 55–63. [CrossRef]
15. Stölken, J.; Evans, A. A microbend test method for measuring the plasticity length scale. *Acta Mater.* **1998**, *46*, 5109–5115. [CrossRef]
16. Barretta, R.; Fabbrocino, F.; Luciano, R.; de Sciarra, F.M.; Ruta, G. Buckling loads of nano-beams in stress-driven nonlocal elasticity. *Mech. Adv. Mater. Struct.* **2020**, *27*, 869–875. [CrossRef]
17. Eringen, A.; Edelen, D. On nonlocal elasticity. *Int. J. Eng. Sci.* **1972**, *10*, 233–248. [CrossRef]
18. Trovalusci, P. *Molecular Approaches for Multifield Continua: Origins and Current Developments*; Springer: Berlin, Germany, 2014; pp. 211–278.
19. Eringen, A.C. On differential equations of nonlocal elasticity and solutions of screw dislocation and surface waves. *J. Appl. Phys.* **1983**, *54*, 4703–4710. [CrossRef]
20. Aifantis, E. Update on a class of gradient theories. *Mech. Mater.* **2003**, *35*, 259–280. [CrossRef]
21. Meenen, J.; Altenbach, H.; Eremeyev, V.; Naumenko, K. A Variationally Consistent Derivation of Microcontinuum Theories. *Adv. Struct. Mater.* **2011**, *15*, 571–584.
22. Mindlin, R.; Eshel, N. On first strain-gradient theories in linear elasticity. *Int. J. Solids Struct.* **1968**, *4*, 109–124. [CrossRef]
23. Karami, B.; Janghorban, M.; Rabczuk, T. Static analysis of functionally graded anisotropic nanoplates using nonlocal strain gradient theory. *Compos. Struct.* **2019**, *227*, 111249. [CrossRef]
24. Eremeyev, V.; Altenbach, H. *On the Direct Approach in the Theory of Second Gradient Plates*; Springer: Cham, Switzerland, 2015; Volume 45; pp. 147–154.
25. Bacciocchi, M.; Fantuzzi, N.; Ferreira, A. Conforming and nonconforming laminated finite element Kirchhoff nanoplates in bending using strain gradient theory. *Comput. Struct.* **2020**, *239*, 106322. [CrossRef]
26. Barretta, R.; Feo, L.; Luciano, R.; Marotti de Sciarra, F.; Penna, R. Functionally graded Timoshenko nanobeams: A novel nonlocal gradient formulation. *Compos. Part B Eng.* **2016**, *100*, 208–219. [CrossRef]
27. Sahmani, S.; Aghdam, M.M.; Rabczuk, T. Nonlinear bending of functionally graded porous micro/nano-beams reinforced with graphene platelets based upon nonlocal strain gradient theory. *Compos. Struct.* **2018**, *186*, 68–78. [CrossRef]
28. Jamalpoor, A.; Hosseini, M. Biaxial buckling analysis of double-orthotropic microplate-systems including in-plane magnetic field based on strain gradient theory. *Compos. Part B Eng.* **2015**, *75*, 53–64. [CrossRef]
29. Apuzzo, A.; Barretta, R.; Faghidian, S.; Luciano, R.; Marotti de Sciarra, F. Free vibrations of elastic beams by modified nonlocal strain gradient theory. *Int. J. Eng. Sci.* **2018**, *133*, 99–108. [CrossRef]
30. Yang, F.; Chong, A.; Lam, D.; Tong, P. Couple stress based strain gradient theory for elasticity. *Int. J. Solids Struct.* **2002**, *39*, 2731–2743. [CrossRef]
31. Mühlhaus, H.; Oka, F. Dispersion and wave propagation in discrete and continuous models for granular materials. *Int. J. Solids Struct.* **1996**, *33*, 2841–2858. [CrossRef]
32. Leonetti, L.; Greco, F.; Trovalusci, P.; Luciano, R.; Masiani, R. A multiscale damage analysis of periodic composites using a couple-stress/Cauchy multidomain model: Application to masonry structures. *Compos. Part B Eng.* **2018**, *141*, 50–59. [CrossRef]

33. Farajpour, A.; Howard, C.Q.; Robertson, W.S. On size-dependent mechanics of nanoplates. *Int. J. Eng. Sci.* **2020**, *156*, 103368. [CrossRef]

34. Barretta, R.; Faghidian, S.A.; Marotti de Sciarra, F. Stress-driven nonlocal integral elasticity for axisymmetric nano-plates. *Int. J. Eng. Sci.* **2019**, *136*, 38–52. [CrossRef]

35. Trovalusci, P.; Bellis, M.D.; Ostoja-Starzewski, M. A Statistically-Based Homogenization Approach for Particle Random Composites as Micropolar Continua. *Adv. Struct. Mater.* **2016**, *42*, 425–441.

36. Reccia, E.; De Bellis, M.L.; Trovalusci, P.; Masiani, R. Sensitivity to material contrast in homogenization of random particle composites as micropolar continua. *Compos. Part B Eng.* **2018**, *136*, 39–45. [CrossRef]

37. Fantuzzi, N.; Leonetti, L.; Trovalusci, P.; Tornabene, F. Some Novel Numerical Applications of Cosserat Continua. *Int. J. Comput. Methods* **2018**, *15*, 1850054. [CrossRef]

38. Jankowski, P.; Żur, K.K.; Kim, J.; Reddy, J. On the bifurcation buckling and vibration of porous nanobeams. *Compos. Struct.* **2020**, *250*, 112632. [CrossRef]

39. Ouakad, H.M.; Valipour, A.; Kamil Żur, K.; Sedighi, H.M.; Reddy, J. On the nonlinear vibration and static deflection problems of actuated hybrid nanotubes based on the stress-driven nonlocal integral elasticity. *Mech. Mater.* **2020**, *148*, 103532. [CrossRef]

40. Kim, J.Y. Micromechanical analysis of effective properties of magneto-electro-thermo-elastic multilayer composites. *Int. J. Eng. Sci.* **2011**, *49*, 1001–1018. [CrossRef]

41. Malikan, M.; Uglov, N.S.; Eremeyev, V.A. On instabilities and post-buckling of piezomagnetic and flexomagnetic nanostructures. *Int. J. Eng. Sci.* **2020**, *157*, 103395. [CrossRef]

42. Aboudi, J. Micromechanical analysis of fully coupled electro-magneto-thermo-elastic multiphase composites. *Smart Mater. Struct.* **2001**, *10*, 867–877. [CrossRef]

43. Vinyas, M.; Kattimani, S.C.; Loja, M.A.R.; Vishwas, M. Effect of $BaTiO_3/CoFe_2O_4$ micro-topological textures on the coupled static behavior of magneto-electro-thermo-elastic beams in different thermal environment. *Mater. Res. Express* **2018**, *5*, 125702. [CrossRef]

44. Vinyas, M.; Kattimani, S. Investigation of the effect of BaTiO3/CoFe2O4 particle arrangement on the static response of magneto-electro-thermo-elastic plates. *Compos. Struct.* **2018**, *185*, 51–64. [CrossRef]

45. Yi, S.; Xu, R.; Qin, X.; Wu, H.; Deng, X.; Gao, R.; Wang, Z.; Chen, G.; Cai, W.; Fu, C. Effect of molar ratio on the microstructure, dielectric and electromagnetic properties of BaTiO3/CoFe2O4 ceramic. *Mater. Res. Express* **2019**, *6*, 116317. [CrossRef]

46. P., K.; Shankar, K.; Ganesan, N. Pyroelectric and pyromagnetic effects on behavior of magneto-electro-elastic plate. *Coupled Syst. Mech.* **2013**, *2*. [CrossRef]

47. Bacciocchi, M.; Fantuzzi, N.; Ferreira, A.J.M. Static finite element analysis of thin laminated strain gradient nanoplates in hygro-thermal environment. *Contin. Mech. Thermodyn.* **2020**. [CrossRef]

48. Dastjerdi, S.; Akgöz, B. New static and dynamic analyses of macro and nano FGM plates using exact three-dimensional elasticity in thermal environment. *Compos. Struct.* **2018**, *192*, 626–641. [CrossRef]

49. Chu, F.; Wang, L.; Zhong, Z.; He, J. Hermite radial basis collocation method for vibration of functionally graded plates with in-plane material inhomogeneity. *Comput. Struct.* **2014**, *142*, 79–89. [CrossRef]

50. Wang, L.; Liu, Y.; Zhou, Y.; Yang, F. Static and dynamic analysis of thin functionally graded shell with in-plane material inhomogeneity. *Int. J. Mech. Sci.* **2021**, *193*, 106165. [CrossRef]

51. Kim, J.; Żur, K.K.; Reddy, J. Bending, free vibration, and buckling of modified couples stress-based functionally graded porous micro-plates. *Compos. Struct.* **2019**, *209*, 879–888. [CrossRef]

52. Yapor Genao, F.; Kim, J.; Żur, K.K. Nonlinear finite element analysis of temperature-dependent functionally graded porous micro-plates under thermal and mechanical loads. *Compos. Struct.* **2021**, *256*, 112931. [CrossRef]

53. Żur, K.K. Free vibration analysis of elastically supported functionally graded annular plates via quasi-Green's function method. *Compos. Part B Eng.* **2018**, *144*, 37–55. [CrossRef]

54. Żur, K.K. Free vibration analysis of discrete-continuous functionally graded circular plate via the Neumann series method. *Appl. Math. Model.* **2019**, *73*, 166–189. [CrossRef]

55. Żur, K.K.; Jankowski, P. Multiparametric Analytical Solution for the Eigenvalue Problem of FGM Porous Circular Plates. *Symmetry* **2019**, *11*, 429. [CrossRef]

56. Simões Moita, J.M.; Mota Soares, C.M.; Mota Soares, C.A. Analyses of magneto-electro-elastic plates using a higher order finite element model. *Compos. Struct.* **2009**, *91*, 421–426. [CrossRef]

57. Mohammadimehr, M.; Rostami, R. Bending, buckling, and forced vibration analyses of nonlocal nanocomposite microplate using TSDT considering MEE properties dependent to various volume fractions of $CoFe_2O_4$-$BaTiO_3$. *J. Theor. Appl. Mech.* **2017**, *55*, 853. [CrossRef]

58. Żur, K.K.; Arefi, M.; Kim, J.; Reddy, J. Free vibration and buckling analyses of magneto-electro-elastic FGM nanoplates based on nonlocal modified higher-order sinusoidal shear deformation theory. *Compos. Part B Eng.* **2020**, *182*, 107601. [CrossRef]

59. Karimi, M.; Farajpour, M. Bending and buckling analyses of BiTiO3–CoFe2O4 nanoplates based on nonlocal strain gradient and modified couple stress hypotheses: Rate of surface layers variations. *Appl. Phys. A* **2019**, *125*. [CrossRef]

60. Arefi, M.; Zenkour, A.M. Thermo-electro-mechanical bending behavior of sandwich nanoplate integrated with piezoelectric face-sheets based on trigonometric plate theory. *Compos. Struct.* **2017**, *162*, 108–122. [CrossRef]

61. Ke, L.L.; Wang, Y.S.; Yang, J.; Kitipornchai, S. Free vibration of size-dependent magneto-electro-elastic nanoplates based on the nonlocal theory. *Acta Mech. Sin.* **2014**, *30*, 516–525. [CrossRef]
62. Gholami, R.; Ansari, R.; Gholami, Y. Size-dependent bending, buckling and vibration of higher-order shear deformable magneto-electro-thermo-elastic rectangular nanoplates. *Mater. Res. Express* **2017**, *4*, 065702. [CrossRef]
63. Ansari, R.; Gholami, R. Size-Dependent Buckling and Postbuckling Analyses of First-Order Shear Deformable Magneto-Electro-Thermo Elastic Nanoplates Based on the Nonlocal Elasticity Theory. *Int. J. Struct. Stab. Dyn.* **2017**, *17*, 1750014. [CrossRef]
64. Ansari, R.; Gholami, R. Nonlocal free vibration in the pre- and post-buckled states of magneto-electro-thermo elastic rectangular nanoplates with various edge conditions. *Smart Mater. Struct.* **2016**, *25*, 095033. [CrossRef]
65. Lei, Z.; Liew, K.; Yu, J. Buckling analysis of functionally graded carbon nanotube-reinforced composite plates using the element-free kp-Ritz method. *Compos. Struct.* **2013**, *98*, 160–168. [CrossRef]
66. Mota, A.F.; Loja, M.A.R.; Barbosa, J.I.; Rodrigues, J.A. Porous Functionally Graded Plates: An Assessment of the Influence of Shear Correction Factor on Static Behavior. *Math. Comput. Appl.* **2020**, *25*, 25. [CrossRef]
67. Brischetto, S.; Leetsch, R.; Carrera, E.; Wallmersperger, T.; Kröplin, B. Thermo-Mechanical Bending of Functionally Graded Plates. *J. Therm. Stress.* **2008**, *31*, 286–308. [CrossRef]
68. Brischetto, S.; Carrera, E. Coupled Thermo-Electro-Mechanical Analysis of Smart Plates Embedding Composite and Piezoelectric Layers. *J. Therm. Stress.* **2012**, *35*, 766–804. [CrossRef]
69. Yan, J.; Tong, L.; Li, C.; Zhu, Y.; Wang, Z. Exact solutions of bending deflections for nano-beams and nano-plates based on nonlocal elasticity theory. *Compos. Struct.* **2015**, *125*, 304–313. [CrossRef]
70. Malikan, M.; Eremeyev, V.A.; Żur, K.K. Effect of Axial Porosities on Flexomagnetic Response of In-Plane Compressed Piezomagnetic Nanobeams. *Symmetry* **2020**, *12*, 1935. [CrossRef]
71. Zhou, L.; Li, X.; Li, M.; Żur, K.K. The smoothed finite element method for time-dependent mechanical responses of MEE materials and structures around Curie temperature. *Comput. Methods Appl. Mech. Eng.* **2020**, *370*, 113241. [CrossRef]
72. Zhou, L.; Nie, B.; Ren, S.; Żur, K.K.; Kim, J. On the hygro-thermo-electro-mechanical coupling effect on static and dynamic responses of piezoelectric beams. *Compos. Struct.* **2020**, 113248. [CrossRef]
73. Tocci Monaco, G.; Fantuzzi, N.; Fabbrocino, F.; Luciano, R. Critical Temperatures for Vibrations and Buckling of Magneto-Electro-Elastic Nonlocal Strain Gradient Plates. *Nanomaterials* **2021**, *11*, 87. [CrossRef]
74. Reddy, J. *Mechanics of Laminated Composite Plates and Shells: Theory and Analysis*, 2nd ed.; CRC Press: Boca Raton, FL, USA, 2003.
75. Tocci Monaco, G.; Fantuzzi, N.; Fabbrocino, F.; Luciano, R. Hygro-thermal vibrations and buckling of laminated nanoplates via nonlocal strain gradient theory. *Compos. Struct.* **2020**, 113337. [CrossRef]
76. Wang, Q. On buckling of column structures with a pair of piezoelectric layers. *Eng. Struct.* **2002**, *24*, 199–205. [CrossRef]
77. Cornacchia, F.; Fantuzzi, N.; Luciano, R.; Penna, R. Solution for cross- and angle-ply laminated Kirchhoff nano plates in bending using strain gradient theory. *Compos. Part B Eng.* **2019**, *173*, 107006. [CrossRef]